U. S. ARMY
TRANSPORTATION RESEARCH COMMAND
FORT EUSTIS, VIRGINIA

TCREC Technical Report 62-2

DUCTED PROPELLER STUDY

Task 9R38-11-009-12

Contract DA 44-177-TC-626

January 1962

prepared by :

EASTERN RESEARCH GROUP
New York, New York

2494-60

DDC AVAILABILITY NOTICES

1. Distribution of this document is unlimited.

2. This document is subject to special export controls and each transmittal to foreign governments or foreign nationals may be made only with prior approval of US Army Aviation Materiel Laboratories, Fort Eustis, Virginia 23604.

3. In addition to security requirements which must be met, this document is subject to special export controls and each transmittal to foreign governments or foreign nationals may be made only with prior approval of USAAVLABS, Fort Eustis, Virginia 23604.

4. Each transmittal of this document outside the agencies of the US Government must have prior approval of US Army Aviation Materiel Laboratories, Fort Eustis, Virginia 23604.

5. In addition to security requirements which apply to this document and must be met, each transmittal outside the agencies of the US Government must have prior approval of US Army Aviation Materiel Laboratories, Fort Eustis, Virginia 23604.

6. Each transmittal of this document outside the Department of Defense must have prior approval of US Army Aviation Materiel Laboratories, Fort Eustis, Virginia 23604.

7. In addition to security requirements which apply to this document and must be met, each transmittal outside the Department of Defense must have prior approval of US Army Aviation Materiel Laboratories, Fort Eustis, Virginia 23604.

8. This document may be further distributed by any holder only with specific prior approval of US Army Aviation Materiel Laboratories, Fort Eustis, Virginia 23604.

9. In addition to security requirements which apply to this document and must be met, it may be further distributed by the holder only with specific prior approval of US Army Aviation Materiel Laboratories, Fort Eustis, Virginia 23604.

DISCLAIMER

10. The findings in this report are not to be construed as an official Department of the Army position unless so designated by other authorized documents.

11. When Government drawings, specifications, or other data are used for any purpose other than in connection with a definitely related Government procurement operation, the United States Government thereby incurs no responsibility nor any obligation whatsoever; and the fact that the Government may have formulated, furnished, or in any way supplied the said drawings, specifications, or other data is not to be regarded by implication or otherwise as

in any manner licensing the holder or any other person or corporation, or conveying any rights or permission, to manufacture, use, or sell any patented invention that may in any way be related thereto.

12. Trade names cited in this report do not constitute an official endorsement or approval of the use of such commercial hardware or software.

DISPOSITION INSTRUCTIONS

13. Destroy this report when no longer needed. Do not return it to originator.

14. When this report is no longer needed, Department of the Army organizations will destroy it in accordance with the procedures given in AR 380-5.

SUMMARY

Various aspects of ducted propeller theory and design are considered. These include the lift of a moderately inclined ducted propeller, possibilities for increasing the static thrust, the related blading design and flow field analysis of interference with adjoining wings or bodies.

The inclined duct theory is shown in agreement with several sets of test data from different sources.

Large static thrust/horsepower values with low jet velocities are predicted for designs which accelerate the inflow in accordance with specified pressure changes inside the duct. These considerations are at present without experimental verification. For such flows, a range of appropriate blading designs are shown by means of solidity, pitch distribution, jet velocity and tip speed.

Digital computer studies are recommended to evaluate favorable and unfavorable interference flow arrangements between ducted systems and surrounding surfaces. The fan-in-wing flow field with a jet of finite size is one of many cases which can be handled. ( )

Task 9R38-11-009-12
Contract DA 44-177-TC-626

January 1962

DUCTED PROPELLER STUDY

by

L. Meyerhoff
P. Zvengrowski

Prepared by:

EASTERN RESEARCH GROUP
120 Wall Street
New York 5, N.Y.

for

U.S. Army Transportation Research Command
Fort Eustis, Virginia

ERG Doc. 947

FOREWORD

The research on which this report is based was performed by the authors, Dr. Leonard Meyerhoff and Mr. Peter Zvengrowski of the Eastern Research Group, New York, New York, under Army contract DA 44-177-TC-626, Task 9R38-11-009-12. The U. S. Army Transportation Research Command (USATRECOM), Fort Eustis, Virginia, was the monitoring agency. This work represents a part of a research program which has been devoted to an investigation of the aerodynamics of shrouded propellers for the purpose of providing design information on a possible means of increasing the static thrust or decreasing the diameter of propellers for V/STOL aircraft. This report is one of several published under the same task.

The report has been reviewed by USATRECOM and is published for the exchange of information and the stimulation of ideas.

FOR THE COMMANDER:

APPROVED BY:

Robert R. Graham
ROBERT R. GRAHAM
USATRECOM Project Engineer

Earl A. Wirth
EARL A. WIRTH
CWO-4 USA
Adjutant

TABLE OF CONTENTS

		Page
	SUMMARY	i
I.	LIFT ON AN INCLINED DUCTED PROPELLER	1
	A. General	1
	B. Lift of a Moderately Inclined Ducted Propeller	3
	C. Comparison with Test Data	6
	1. Comparison with experimental data from Ref. 7	7
	2. Comparison including the effect of jet contraction	10
	3. Comparison with experimental data from Ref. 8	13
	4. Comparison with experimental data from Ref. 9	17
	D. Concluding Notes	21
II.	POSSIBLE STATIC THRUST IMPROVEMENT	23
	A. Relation of Thrust to Thrust/Horsepower Ratio	23
	B. Flow Values for Large Jet Area	25
	C. Numerical Example	29
III.	BLADING DESIGN CONSIDERATIONS	33
IV.	ADDITIONAL DESIGN CONSIDERATIONS	41
	A. Duct	41
	B. Tip Clearance Losses	42
	C. Possible Propulsive Efficiency Improvement	43
V.	FLOW FIELD STUDIES	45
	A. General	45
	B. Analysis	46
	C. Concluding Notes	56
VI.	APPENDIX	57
VII.	SYMBOLS	61
	Subscripts	62
VIII.	LIST OF FIGURES	63
IX.	BIBLIOGRAPHY	65
X.	REFERENCES	66

SUMMARY

Various aspects of ducted propeller theory and design are considered. These include the lift of a moderately inclined ducted propeller, possibilities for increasing the static thrust, the related blading design and flow field analysis of interference with adjoining wings or bodies.

The inclined duct theory is shown in agreement with several sets of test data from different sources.

Large static thrust/horsepower values with low jet velocities are predicted for designs which accelerate the inflow in accordance with specified pressure changes inside the duct. These considerations are at present without experimental verification. For such flows, a range of appropriate blading designs are shown by means of solidity, pitch distribution, jet velocity and tip speed.

Digital computer studies are recommended to evaluate favorable and unfavorable interference flow arrangements between ducted systems and surrounding surfaces. The fan-in-wing flow field with a jet of finite size is one of many cases which can be handled.

I. LIFT ON AN INCLINED DUCTED PROPELLER

A. General

It is well known that a duct of length L and inner diameter d inclined at angle α to an oncoming flow produces a lift force. The lifting characteristic of the inclined duct (ring-wing) is similar to that of the conventional planar wing; this is seen from the aspect ratio type of effect dependent on L/d and the lift-drag polar.*

Analytical studies now enable prediction of the lift curve and the dependency on L/d to a degree quite useful for engineering prediction.** This is demonstrated in REF. 1. It is worth noting that the use of the inner diameter of the duct, for ducts of finite thickness ratios, seems to provide the favorable agreement between theory and experiment. These results are established for ducts of essentially constant inner diameter. Similar developments for ducts having appreciable inner contour change are not clearly evident in the literature.

With the introduction of an operating propeller inside the duct the lifting characteristics become different from the unpowered duct. From an elementary viewpoint this is seen from the larger vertical flow (jet)

---

* REF. 1 Experimental Investigation of Lift, Drag and Pitching Moment of Five Annular Airfoils by H.S. Fletcher, NACA TN 4117. 1957.

** REF. 2 The Ring Airfoil in Nonaxial Flow, by H.S. Ribner Jour. Aero. Sci., Vol. 14, 1947, page 529.

REF. 3 Etude Theorique De L'Aile Annulaire by M.G. Faure. Technique Et. Science Aeronautique. Tome 6, 1956.

REF. 4 Zur Aerodynamic des Ringflugels by J. Weissinger, DVL Bericht Nr. 2, 1955.

momentum component of the powered versus the unpowered duct. REF. 5, for example, uses this type of approach together with empirical factors to develop a method to predict the lift force.

A lift dependence on L/d for the powered duct can also be anticipated. The extent that the lift departs from the vertical component of jet momentum depends on L/d. For example, a jet engine enclosed in a nacelle will have an L/d value in the order of 3; inclining the engine, at relatively low airspeeds, yields a lift force very close to the vertical jet exit momentum component. With the introduction of the ducted-fan jet engine, the enclosing nacelle shows smaller L/d values and it can be anticipated that the interaction of internal and exit flows will produce vertical forces greater than the jet momentum component. An introductory treatment of the effect of duct length/diameter ratio in relation to interference effects between duct and jet flow is given in REF. 6. Increasingly large L/d values lead to smaller interaction effects.

In the next section, available test data on moderately inclined powered ducts are compared with an analytical procedure based on flow through nonpowered ducts.

REF. 5 Performance Calculation of Aerodyne Systems in Cruising Flight by A.M. Lippisch. Collins Radio Company Rept. Cer-617, 1957. Confidential

REF. 6 An Estimate of the Forces on Annular Fairings by J.A. Bagley. Jour. Roy. Aero. Soc., vol. 63, 1959, page 315.

B. Lift of a Moderately Inclined Ducted Propeller

Details of the method are described in Appendix A. This method, as shown, extends the vortex theory of an unpowered duct to take account of the induced effects of the jet vorticity.

For the unpowered duct the lift coefficient $C_{L,u}$ is given by

$$C_{L,u} = C_{L_\alpha} (\alpha^o/57.3) \tag{1}$$

where C_{L_α} is the lift curve slope dependent on the duct length diameter ratio. Referenced papers present different methods for deriving the lift curve slope. For simplicity the curve given in REF. 1 can be taken in the approximating form:

$$C_{L_{\alpha,u}} = [.0547/(L/d)-.0063]/(L/d)^2 . \tag{2}$$

Using this relation for the lift curve slope, the derivation of Appendix A shows the lift coefficient, $C_{L,p}$ for the duct with an operating ducted propeller; namely:

$$C_{L,p} = \{[.25C_{L_\alpha}(V_1/V+1)^2] + (.5\pi/\lambda)[(V_j/V)(V_1/V)-1]\}\alpha^o/57.3 \tag{3}$$

where V_1 is the averaged velocity inside the ducted system.
V is the advance speed.
V_j is the jet velocity.
λ is L/d.

Without power, the theory requires $V_1 = V$ and $V_j = V$, and Eq. 3 reduced to Eq. 1 for these velocity values.

An indication of the effect of power on the lift curve slope can be had by setting $V_1/V = 1.0$ in Eq. 3 and inserting Eq. 2 for the unpowered $C_{L_{\alpha,}}^{\circ}$; the result becomes

$$\frac{C_{L_{\alpha,p}}}{C_{L_{\alpha,u}}} = 1 + (.5\pi/\lambda)(V_j/V-1)/C_{L_{\alpha,u}} \tag{4}$$

and is plotted on FIG. 1 with the thrust coefficient C_T as abscissa; the definition of C_T is

$$C_T = T/(1/2)\rho V^2 \; A_{ex} \tag{5}$$

where A_{ex} is the exit area of the duct. For the assumption that the ultimate jet area $A_j = A_{ex}$, it follows that for a radially averaged flow

$$C_T = 2(V_j/V)(V_j/V-1) \tag{6}$$

based on the thrust

$$T = \rho A_j V_j (V_j - V). \tag{7}$$

FIG. 1 shows a large increase for the lift slope curve with increasing thrust coefficient. Decreasing L/d ratio also increases the lift curve slope. For L/d values of 0.6 and greater the effect of L/d becomes much smaller. The valid extent of FIG. 1 depends on the closeness of A_e to A_j. With increasing thrust coefficients, it is most likely the jet contracts downstream of the exit plane. Jet contraction probably is a secondary effect for thrust coefficients of 1.0 and below.

FIG. 1 is based on $V_1/V = 1.0$; larger lift slope curves will occur for designs having $V_1/V>1.0$.

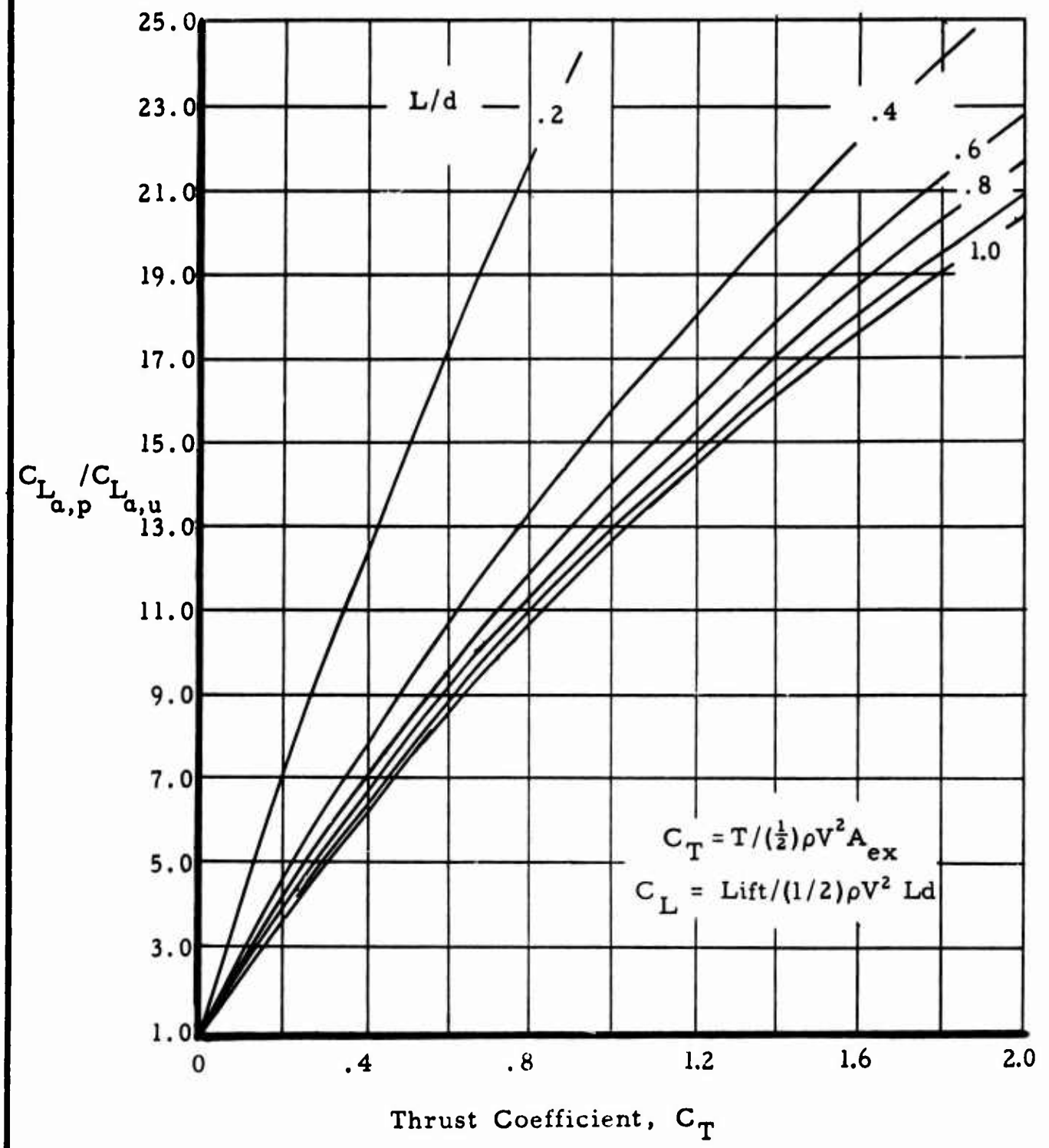

FIG. 1 RATIO OF LIFT CURVE SLOPES FOR POWERED AND UNPOWERED DUCTS

C. Comparison with Test Data

Eqs. 1 and 3 will be compared with data in REFS. 7, 8 and 9.* In order to compare theory with experiment, it is necessary to know flow velocities at the duct. Such data are not available for the referenced experiments and the procedure outlined below is followed for estimating the jet velocity.

The power input to the flow (ft.-lb./sec.) according to kinetic energy principles is;

$$P = (1/2)\rho A_j V^3 (V_j/V)[(V_j/V)^2 - 1] k_L \qquad (8)$$

where V is the free stream velocity.

V_j is the jet velocity.

A_j is the jet cross section area.

k_L is a loss function greater than 1.0; for zero loss, $k_L = 1.0$.

The propulsive efficiency of the ducted system from momentum consideration is:

$$e_p = 2/[k_L(V_j/V + 1)] \qquad (9)$$

where, as above, k_L takes account of losses through the blading.

---

* REF. 7 Shrouded Propeller Investigations: Wind Tunnel Tests of a Shrouded Propeller with a 10-Bladed Propeller, Exit Stators and Long Chord Shroud With High Speed Inlet and No Exit Diffusion by V.O. Hoehne. Univ. of Witchita, Engrg. Rept. No. 213-5, Jan. 1959.

REF. 8 Wind Tunnel Test of Several Ducted Propellers In Non-Axial Flow by W. J. Gill, Hiller Aircraft Rept. No. ARD-224, April 1957.

REF. 9 Wind Tunnel Tests of Shrouded Propellers At Mach Numbers From 0 to 0.60 by R.M. Grose. WADC TR 58-604. December 1958.

Eliminating k_L between Eqs. 8 and 9 yields:

$$(V_j/V)[(V_j/V)-1] = Pe_p/\rho A_j V^3 \ . \tag{10}$$

The right side of Eq. 10 containe P and e_p which are obtainable from the test data; jet area A_j can be approximated by the duct exit area, provided the jet does not contract greatly. The effect of jet contraction is considered later.

1. <u>comparison with the experiment data (REF. 7)</u>

REF. 7 presents thrust and power data in terms of coefficients defined by

$$\begin{aligned} C_N &= F_n/\rho V^2 \ d^2 \\ T_c &= T/\rho V^2 \ d^2 \\ P_c &= P/\rho V^3 \ d^2 \end{aligned} \tag{11}$$

FIG. 2 illustrates the relation between the force data C_N, T_c and the lift coefficient C_L.

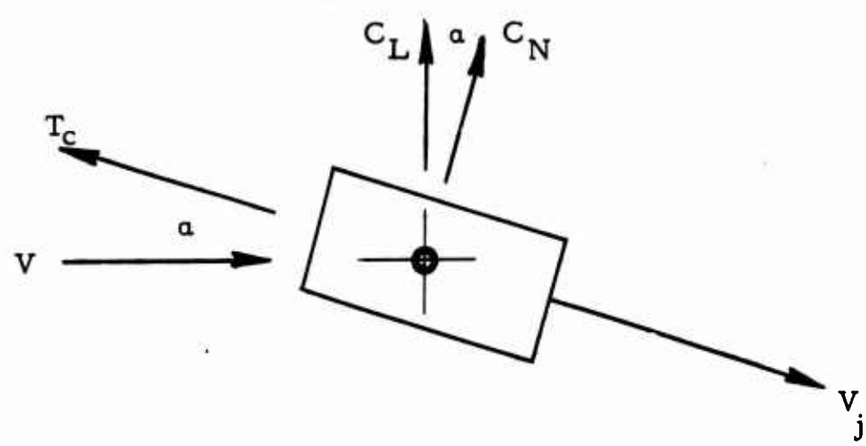

FIG. 2 GEOMETRY OF FORCES

It is seen from FIG. 2 that

$$C_L = C_N \cos \alpha + T_c \sin \alpha. \tag{12}$$

The geometry of the ducted system in REF. 7 is as follows:

a) propeller diameter, 13.92 inches.
b) hub diameter, 4.76 inches ($d_h/d = .3$).
c) exit diameter, 13.92 inches.
d) duct length, 9.526 inches.
e) $L/d = .684$.
f) exit area is reduced 5.7% due to support fairing.

TABLE I lists the test data to which Eq. 3 will be compared.

TABLE I

Test Data From REF. 7

(light loading)

α^o	J_o	β @ .8R	P_c	T_c	e_p	C_N	$C_N \cos\alpha$	$T_c \sin\alpha$	Eq. 12 $C_{L,p}$
0	1.35	42.5	.5	.34	.678	0	0	0	0
10	1.35	42.5	.5	.34	.678	.3	.296	.059	.355
20	1.35	42.5	.5	.34	.678	.6	.564	.116	.680
30	1.35	42.5	.5	.34	.678	.8	.693	.170	.863

$\alpha = o°$

Inserting the geometrical and experimental data into Eq. 10 yields

$$V_j/V = 1.36$$

$$V_1/V = 1.28 \text{ (from flow continuity).} \tag{13}$$

These values, together with Eq. 3 yield the theoretically determined value of $C_{L,p}$. FIG. 3 compares theory and experiment. Also shown on FIG. 3 is the lift curve for the unpowered duct.

Theory is shown on FIG. 3 to furnish a correct guide to the physical situation of this isolated set of test data; for moderate angle of attacks the theory furnishes a good engineering approximation despite the simplfying assumptions involved. The addition of power appears to increase lift about 100% within the unstalled range; this ratio may persist even to the higher angle of attack range provided the lift curve slope of the unpowered duct decreases similarly to that of the powered duct.

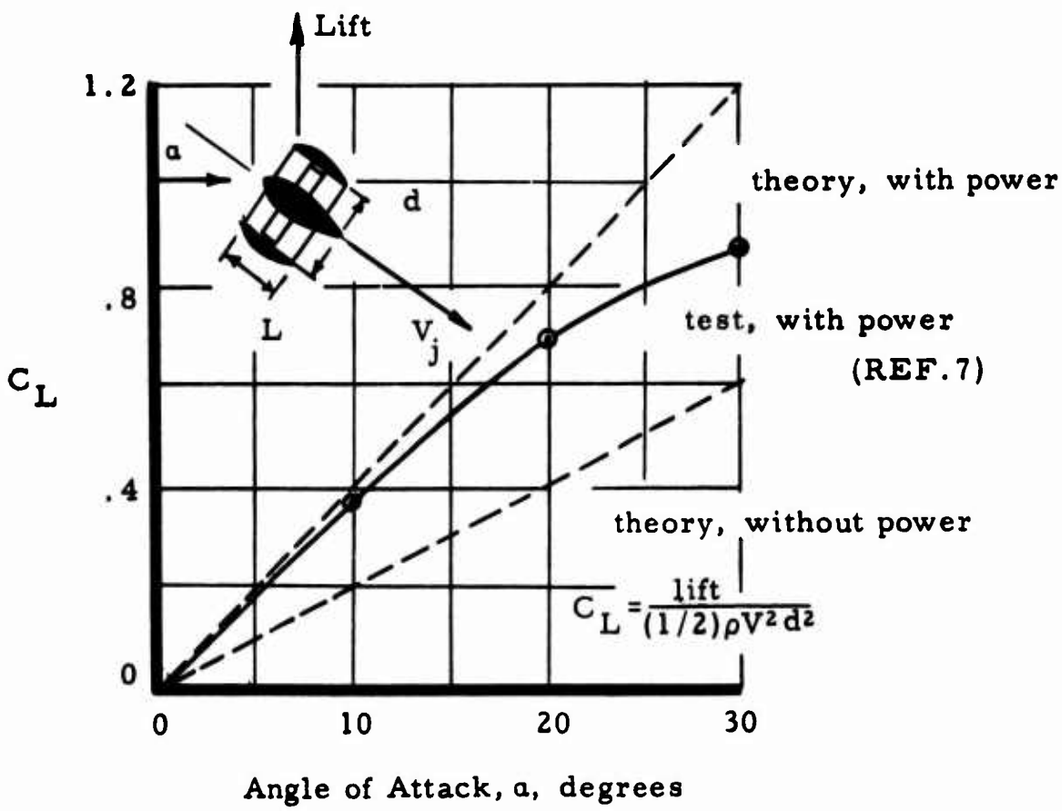

FIG. 3 LIFT OF INCLINED DUCT (L/d = .684)

2. Comparison with REF. 7 including the effect of jet contraction

The foregoing comparison of lift coefficients is made for a ducted system with a relatively low thrust loading. This comparison requires an estimate of the jet cross-section area; in view of the light-loading conditions, a jet area the same as ducted propeller exit area is assumed. While this choice is reasonable for a lightly loaded system it should not be expected to apply generally for a highly loaded ducted propeller having an exit area the same as the propeller disk area. The test data of REF. 7 are obtained from a ducted system with only a slight duct contraction between propeller disk and exit plane due to support struts. Hence, for much higher thrust loadings, the flow leaving the duct must be presumed to return the equilibrium downstream of the duct by an externally contracting jet. In order to compare theory and experiment for duct lift for higher thrust loadings at low propeller advance ratios, an estimate is needed of the jet area.

To illustrate further the nature of this problem, consider the contracting jet at the duct exit as shown on FIG. 4.

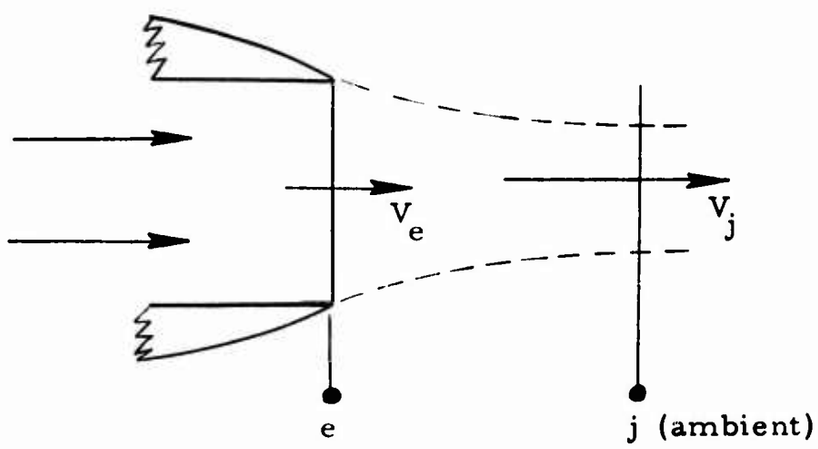

FIG. 4 CONTRACTING JET

Bernoulli's equation between stations e and j, together with the corresponding continuity relation, yields, for an incompressible fluid,

$$A_e/A_j = \sqrt{1 + (p_e - p_j)/(1/2)\rho V_e^2} \tag{14}$$

which allows an estimate of the contracted jet area, provided the overpressure is known at the duct exit; this pressure can be predicted by an iterative procedure for calculating the pressure rise across the propeller for a prescribed power input and advance ratio. The interacting effect of the duct on the inflow at the rotor is an added complication. One general approach is to calculate this pressure rise at each blade radius by a 'strip' method taking account of duct interaction. From the pressure rise and duct cross-section areas, the pressure at the duct exit can be estimated. This can be a lengthy procedure and for the purpose of predicting duct lift at low advance ratios an approximate method will be attempted as described below.

It is assumed the streamtube, starting from the duct exit, contracts similarly to the jet of a free propeller having the same mass flow and ultimate jet velocity. The actuator disk-momentum method, it will be recalled, gives the velocity through the disk of a free propeller as the average of upstream and downstream velocities. For the contracting jet leaving the duct exit, the above assumption requires the duct exit velocity to be the average of upstream and downstream velocities. That is, by continuity of flow

$$A_j/A_e = V_e/V_j = (1+V_j/V)/2(V_j/V) \tag{15}$$

which furnishes an equation for the additional variable A_j. The comparison between theory and experiment for powered duct lift can now follow the method applied earlier. A convenient modification of this method can be based on calculating the jet velocity from thrust data given by the coefficient T_c (relations 11):

$$T = \rho V^2 d^2 T_c = \rho A_j V_j (V_j - V) \tag{16}$$

together with Eq. 15 for A_j, it follows that

$$V_j/V = \sqrt{1 + 2d^2 \; T_c/A_e} \tag{17}$$

from which the jet velocity can be estimated for a jet contracting downstream of the duct exit.

For the duct geometry of REF. 7 shown on page 8, Eq. 17 becomes

$$V_j/V = \sqrt{1 + 2.967 \; T_c}. \tag{18}$$

In addition, the internal velocity V_1/V is also required by Eq. 3 for the powered lift. From the continuity of flow between propeller and exit for the design of REF. 7, the following ratio applies:

$$V_1/V_e = .943 \tag{19}$$

and from the exit station to the ultimate jet

$$V_1/V_e = .943(A_j/A_e)(V_j/V). \tag{20}$$

Test data from REF. 7 (J, T_c and C_{L_p}) for varying advance ratios are shown on TABLE II.

TABLE II

Test (REF.7) and Calculated data
varying loadings

J	T_c	C_{L_p}	V_j/V	V_1/V	A_j/A_e
.3	11.5	2.87	5.93	3.27	.58
.5	3.75	1.24	3.48	2.11	.64
.8	1.18	.59	2.12	1.47	.74
1.2	.37	.36	1.45	1.15	.85
			Eq. 18		Eq. 15

Also shown on TABLE II are flow and area ratios computed by the foregoing method.

FIG. 5 compares theory and experiment. At low advance ratios the approximation for the jet area permits closer agreement with the tests than the assumption of a noncontracting jet. As the advance ratio increases it is also seen that the assumption of a noncontracting jet yields closer agreement with test data.

FIG. 6 is a plot of the test data J vs T_c; FIG. 7 shows A_j/A_{ex} versus the thrust coefficient T_c. For comparison with the values on FIG. 7, it may be recalled that the momentum theory for a free propeller yields jet area ratios between 1.0 and 0.5 for zero and static thrusts, respectively. More work is needed on the nature of the interacting flow fields due to the duct and the exit flow.

It is interesting to note that the magnitude of the lift coefficients on FIG. 5 results from approximately 65% jet momentum component and 35% circulation effect. These values can be obtained by comparing the vertical jet momentum with the total lift force with power.

3. Comparison with experimental data (REF. 8)

A similar comparison of theory and experiment can be made for the data in REF. 8. For this source, the test data notation are K_L and K_p; the relation of K_L and K_p to the coefficients used previously is:

$$K_L = L/\left[\rho(\omega R)^2 \quad A\right] = C_{L,p}(.5\lambda^2/.25\pi f) \qquad (21)$$

$$K_p = P/\left[\rho(\omega R)^3 \quad A\right] = P_c\ (\lambda^3/.25\pi f)$$

where $\lambda = \omega R$ and $f = 1 - (d_h/d)^2$.

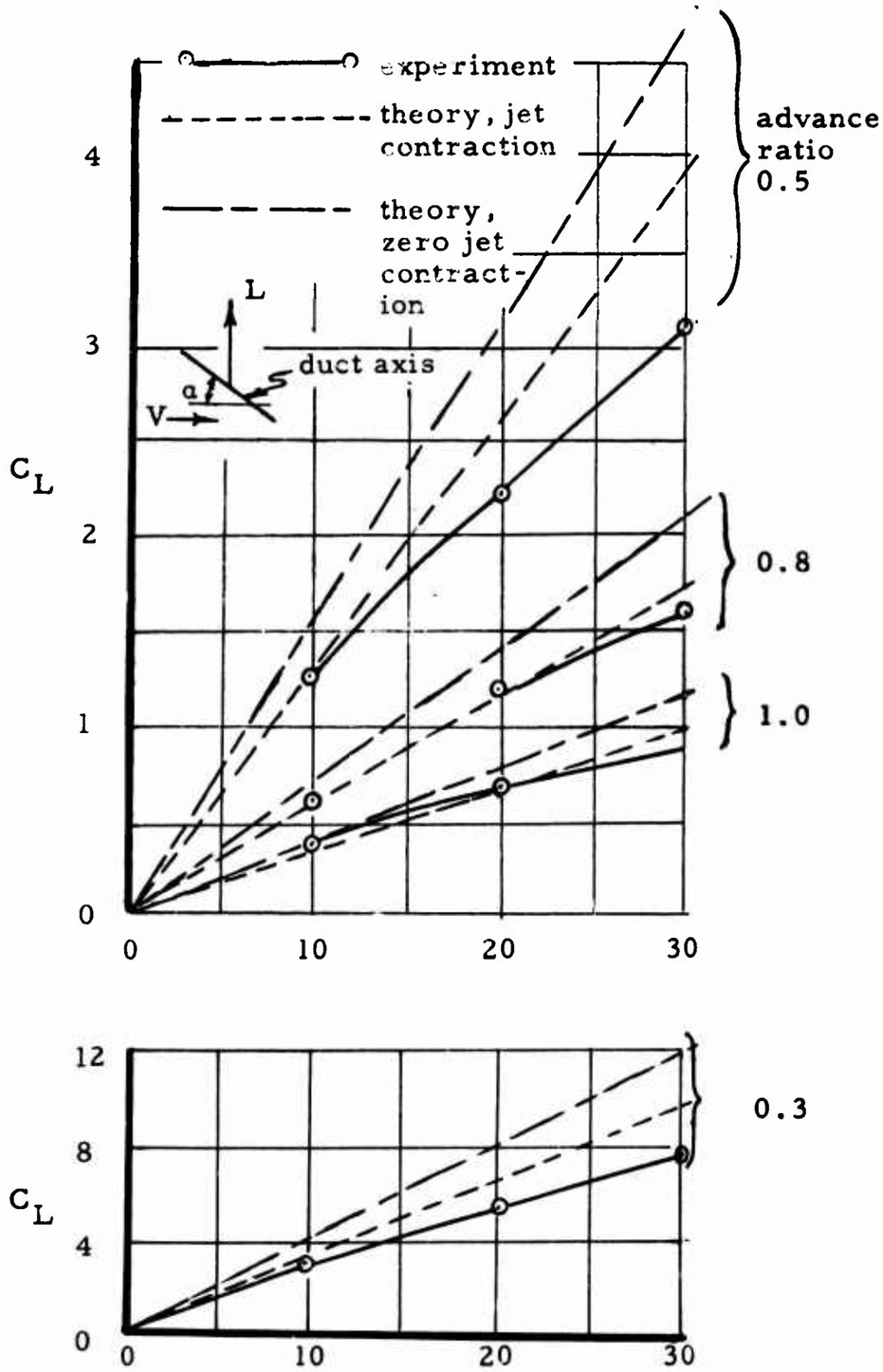

FIG. 5 LIFT OF INCLINED DUCT (L/d = .5) WITH OPERATING PROPELLER

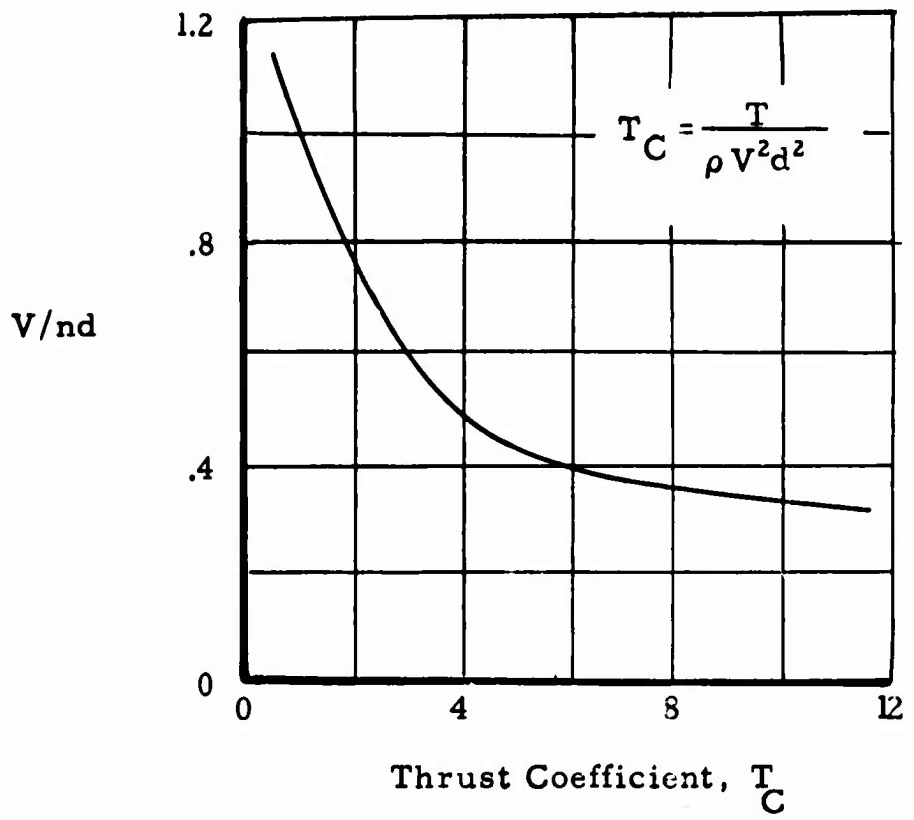

FIG. 6 THRUST COEFFICIENT

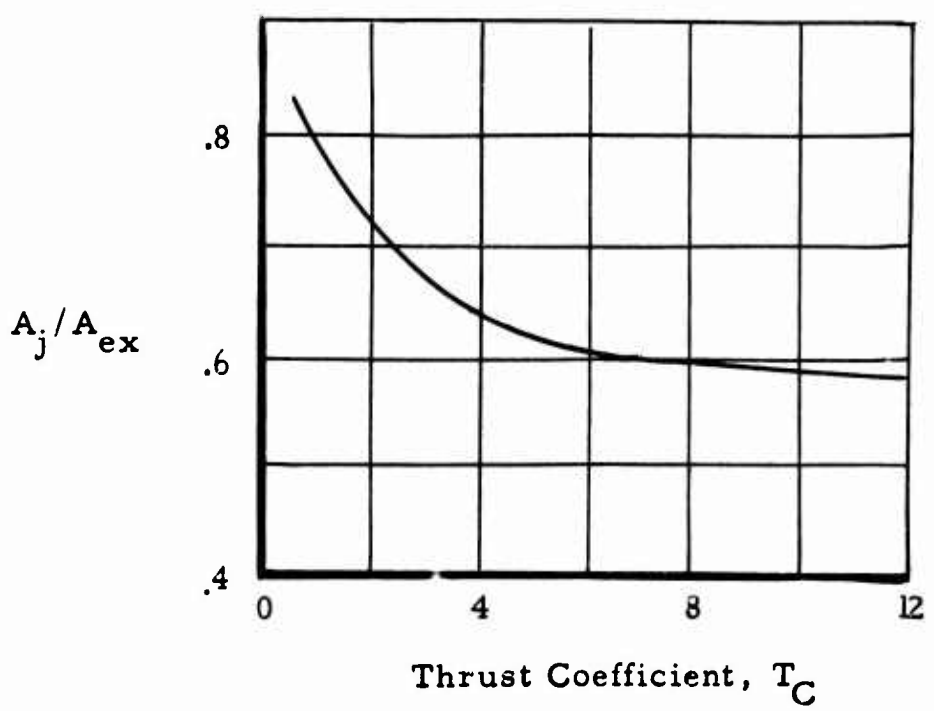

FIG. 7 JET CONTRACTION RATIO

The geometry of the ducted system in REF. 8 is as follows:

a) propeller diameter, 2 feet.
b) hub diameter, 0.43 feet (d_h/d = .215), f = .954.
c) exit diameter, 2 feet.
d) duct length, 6 inches, duct no. $D_1 P_3 S$.
e) L/d = .25.

TABLE III below lists the test data to which Eq. 3 will be compared.

TABLE III

Test data from REF. 8 (Fig. 44a,b)

α	λ	β @ .7R	K_L	K_P	e_p	P_c	$C_{L,p}$
0	.15	9°	.0	.0016	.234	.355	0
10	.15	9°	.0016	.0016	.234	.355	.400
20	.15	9°	.010	.0016	.234	.355	.666
30	.15	9°	.0135	.0016	.234	.355	.899

Eq. 21

Inserting data back into Eqs. 10 and 11 yields

$$V_j/V = 1.10$$
$$V_1/V = 1.10 \qquad (22)$$

which seems to be a low jet velocity value. The ideal momentum efficiency is .95 based on this jet velocity ratio; however, in this region of jet ratios the influence of friction losses predominates and low actual efficiencies occur.* As before, the above values are to be inserted into Eq. 3 to calculate $C_{L,p}$ for comparison. FIG. 8 shows this comparison.

---

* REF. 10 The Flow Over Annular Aerofoils, by D. Kuechmann and J. Weber. G.D.C. 10/1133 T, Ministry of Supply, British.

FIG.8 shows a similar agreement between test and theory as seen on FIG. 3. The duct L/d of the former is .25, and is 0.684 for the latter; hence, the theory, for these isolated cases shows good agreement for a fairly wide range of L/d values.

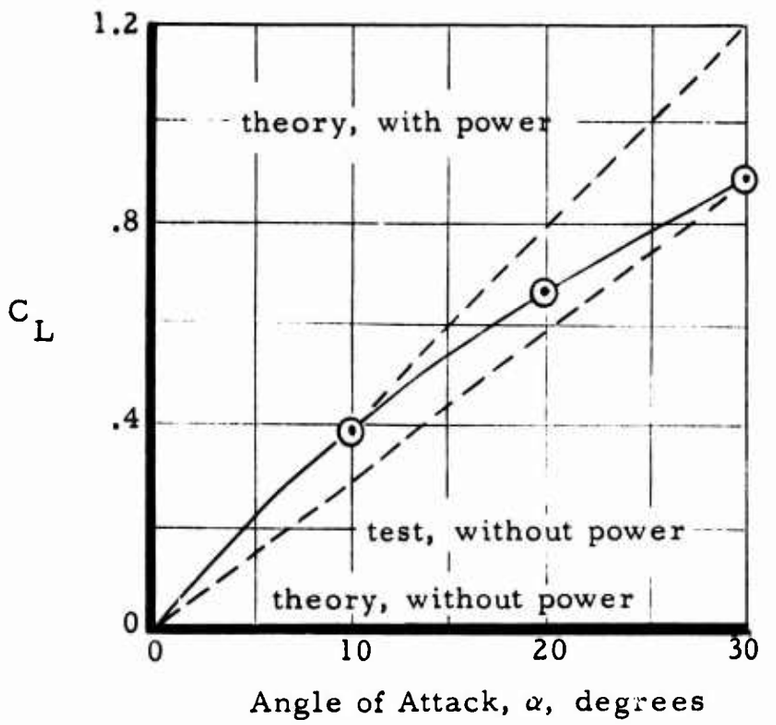

FIG. 8 LIFT OF INCLINED DUCT (L/d = .25)

4. Comparison with the experimental data (REF. 9)

The above data allow an additional correlation between theory and experiment for the inclined ducted propeller. These data are obtained from a system with the following characteristics:

a) propeller diameter, 2.5 feet.
b) hub diameter, .625 feet (d_n/d = .25).

c) annular exit area, 11% greater than at rotor.

d) duct length, 1.25 feet.

e) $L/d = 0.5$.

REF. 9 presents data in terms of the following coefficients

$$C_T = T/\rho n^2 d^4, \text{ thrust}$$
$$C_p = 2\pi Q/\rho n^2 d^5, \text{ power}$$
$$\eta = C_T J/C_p, \text{ efficiency}$$
$$C_L = L/q d_s C_s, \text{ lift}$$

where d_s and C_s are the duct diameter and length respectively. TABLE IV lists the test advance ratio and thrust coefficient at two different blade angles. Corresponding test data on lift versus angle of attack are given on FIG. 9; net efficiency is shown on FIG. 10.

TABLE IV

test data from REF. 9

$\beta = 17^\circ$	
J	C_T
.60	.089
.64	.075
.69	.051
.75	.029

$\beta = 32^\circ$	
J	C_T
.93	.271
1.03	.224
1.23	.135
1.40	.070

The blade angles of 17° and 32° cover the maximum range for the test data at a test speed of Mach 0.2.

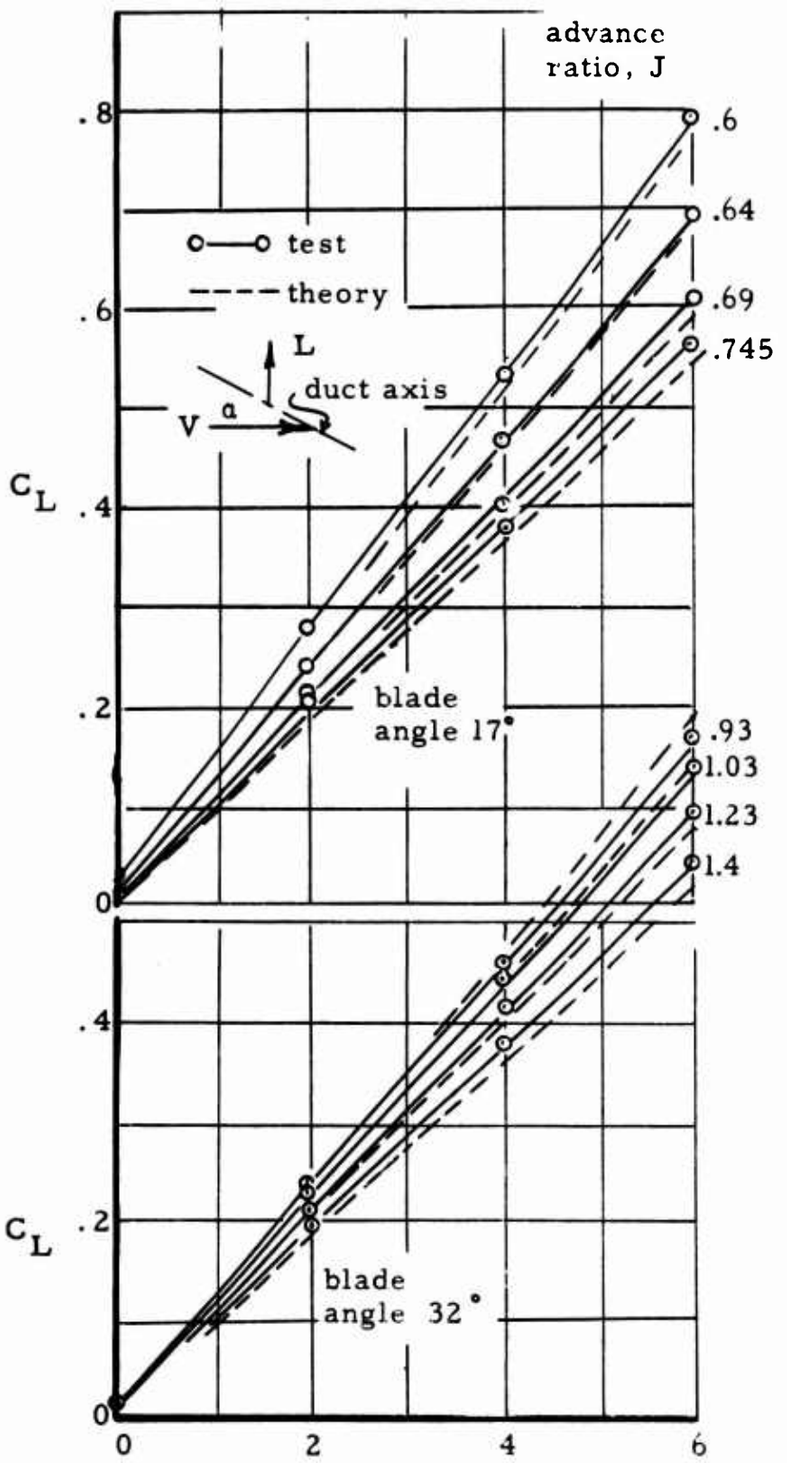

$$C_L = \frac{L}{(\frac{1}{2})\rho V^2 (dL)}$$

FIG. 9 LIFT OF INCLINED DUCT (L/d = .5) WITH OPERATING PROPELLER

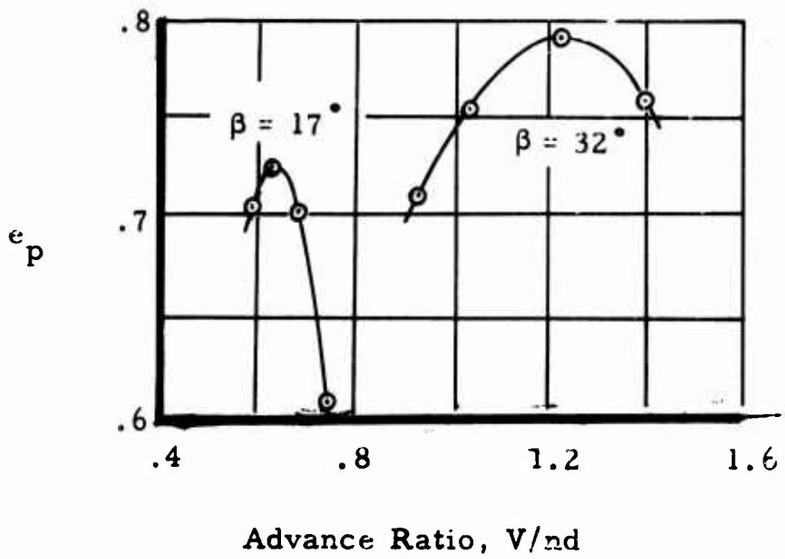

FIG. 10 NET EFFICIENCY OF DUCTED PROPELLER

The procedure for calculating the lift to compare with the test data is the same given before with a contracting jet; namely:

$$T = \rho n^2 d^4 C_T = \rho A_e V_e (V_j - V) \tag{23}$$

where, as before, $V_e/V = .5(1+V_j/V)$; it follows that:

$$V_j/V = \sqrt{1 + 2.448\, C_T/J^2} \tag{24}$$

From this point the procedure is the same as shown previously.

FIG. 9 compares theory and test for the lift coefficient for several advance ratios and the two blade angles. The calculated lift coefficients are seen to be in good agreement with test data.

Efficiency data on FIG. 10 are generally higher than the other data examined earlier. However, the efficiencies on FIG. 10 should be still greater if only considered on the estimated jet velocities obtained from Eq. 24. For example at $\beta = 17^\circ$, the calculated jet velocities vary from 1.43 to 1.08 over the range of advance ratios and from 1.36 to 1.05 at $\beta = 32^\circ$. Ideal efficiencies based on these jet velocities approach 20% higher efficiencies than the test data.

One explanation generally used to explain such a difference is based on the fact that the relative thrust to drag of the system is responsible; that is, lightly loaded ducted systems can experience large reductions in efficiency from the ideal value.

D. Concluding Notes

Three different set of ducted propeller lift data are examined herein relative to theoretical predictions. Agreement is generally good over a wide range of operating conditions. Correlation at low advance ratio need improvement. The behavior of the jet issuing from the duct needs

clarification regarding subsequent contraction or expansion; a calculation of the flow field of ducted propellers with appropriate thrust loadings should provide the needed results concerning the jet. Such a study would also be of use for evaluating the inlet efficiency with a highly convergent inflow relative to the same inlet with less inflow convergence.

II. POSSIBLE STATIC THRUST IMPROVEMENT

A. Relation of Thrust to Thrust/Horsepower Ratio

The problem of improving static thrust can be described by the elementary theory which follows.

The static thrust of a torque-balanced system* in terms of radially averaged flow values is:

$$T = \rho A_j V_j^2 \tag{25}$$

where A_j and V_j are the jet cross section area and velocity respectively, both at ambient pressure. Taking account of the thrust/horsepower ratio from Eq. 25 and 8 (with zero flow losses).

$$\frac{T}{HP} = \frac{1100}{V_j} \tag{26}$$

Eq. 25 becomes:

$$T = \rho A_j \left(\frac{1100}{T/HP}\right)^2 \tag{27}$$

FIG. 11 is a plot of Eq. 27. As seen, it is desirable to have T/HP as large as possible for a specified thrust, as well as the smallest diameter consistent with good overall efficiency.

---

* Whirl velocity component of propeller is removed by a stator-rotor set.

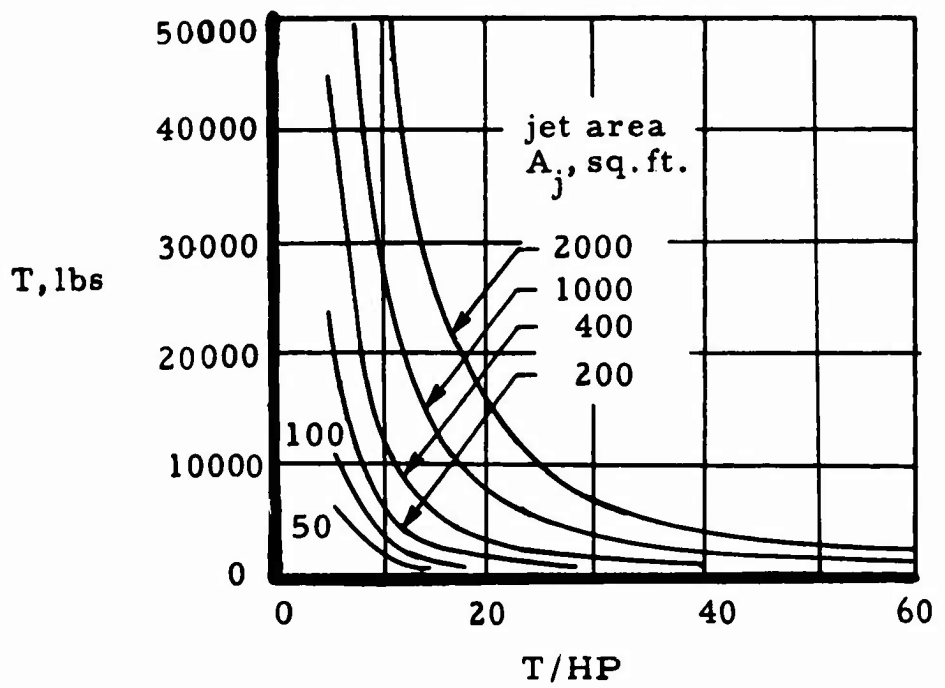

FIG. 11 EFFECT OF THRUST/HORSEPOWER AND JET AREA ON STATIC THRUST

High T/HP values lead to power economy as well as low jet velocities (Eq. 26). FIG. 11 shows large jet areas occur with increasing values of T/HP at a fixed thrust requirement. In principle, the derivation of FIG. 11 does not require a propeller area similar to the jet area; the type of duct and propeller design required by theory to produce a large jet area with a much smaller rotor area will be given shortly.

Existing ducted propeller designs generally show values of rotor disk areas similar to exit disk areas; also, the ultimate jet area usually is ass .med about the same as the exit disk area. With such practice,

a large jet area will require a large propeller diameter. This point will be considered again later.

B. Flow Values for Large Jet Area

A further examination of the foregoing static thrust case is shown on FIG. 12 where the pressure rise Δp_r across the rotor disk is given as a function of T/HP; increasing values of T/HP are seen to require decreasing values of Δp_r.

The derivation of FIG. 12 follows from Bernoulli equation

$$p_o + \Delta p_r = p_j + (1/2)\rho V_j^2 \tag{28}$$

Eq. 26 furnishes a value of V_j; since the jet pressure $p_j = p_o$, Eqs. 26 and 28 yield:

$$\Delta p_r = (1/2)\,\rho\,[\,1100/(T/HP)]^2 \tag{29}$$

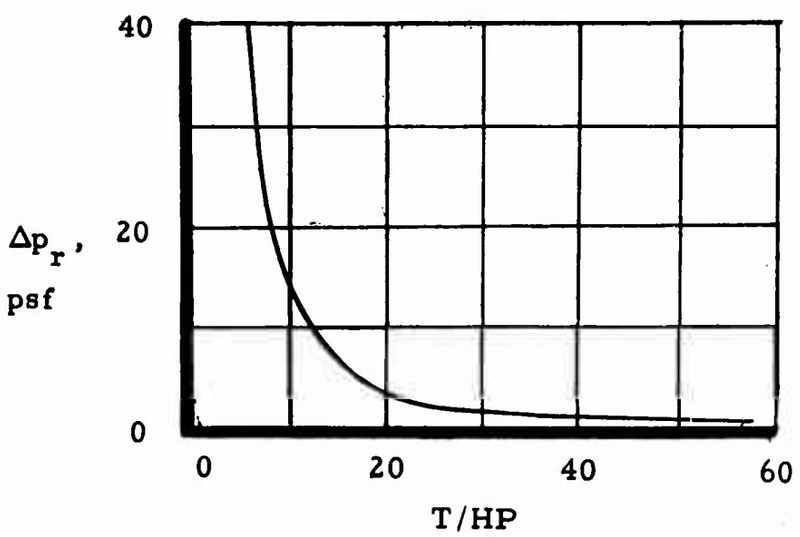

FIG. 12 EFFECT OF THRUST/HORSEPOWER ON ROTOR PRESSURE RISE

Since the thrust on the propeller $\Delta P_r A_p$ decreases with increasing T/HP, (Eq. 29) it is necessary for an increasing axial thrust force to develop on the duct. This is seen from the ideal ratio of duct force F_d to total static thrust T, viz:*

$$\frac{F_d}{T} = 1 - .5 \frac{A_p}{A_j} \tag{30}$$

which is obtained by subtracting the force on the rotor from the net thrust. As seen, the force on the duct increases with increasing jet area.

To summarize, for a given propeller diameter, increasing values of T/HP require increasing jet areas; the pressure rise across the rotor decreases for increasing T/HP-values. Hence, the duct must carry a greater part of the net thrust. FIG. 13 illustrates the type of flow needed.

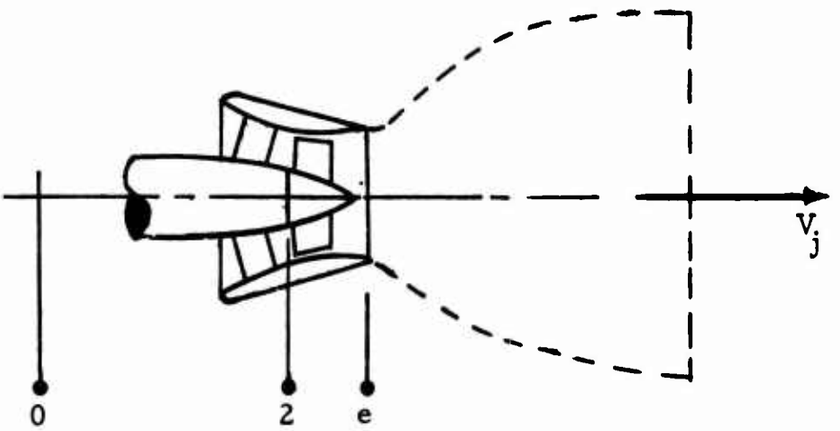

FIG. 13 EXPANDING JET FLOW

---

* The figure of merit of a ducted propeller with an expanding jet is $2\sqrt{A_j/A_p}$; a usually quoted maximum value for a ducted system is 2.0. This figure of merit is defined by $M = (T/P)\sqrt{T/2\,\rho A_p}$.

Available test results on a ducted propeller only consider ducts with internal area expansions; e.g., see REFS. 11 and 12. A rearranged form of the data in REF. 11 is shown on FIG. 14.

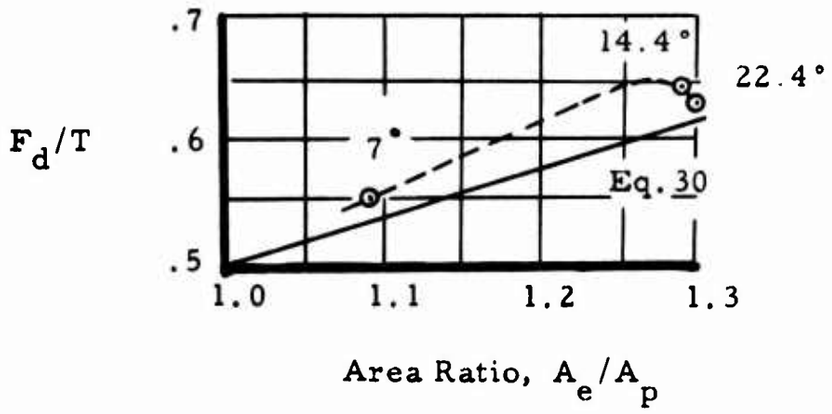

FIG. 14 EFFECT OF INTERNAL AREA RATIO ON DUCT FORCE

Internal expansion angles are given on FIG. 14. These data indicate that flow separation from the duct walls prevented further increase of duct thrust. Area ratios greater than the values on FIG. 14 are postulated by the flow type of FIG. 13. The method of REF. 12 seeks to improve static thrust by large expanding internal exit areas with various flow control means to force the flow to adhere to the expanding duct walls; results do not attain the promise of the theory due to flow diffi-

---

REF. 11 Static Tests of a Shrouded and an Unshrouded Propeller, by R.J. Platt, Jr. NACA RM L7H25. February 1948.

REF. 12 Investigation of Large Expansion Diffusers For Minimum Rotor Area by J.R. Duvivier and R. B. McCallum. Mass. Inst. Tech. Aero and Struct. Res. Lab. T.R.81-1. Nov. 1959.

culties along the duct passageway. Should such flows be feasible whether internal or external flow expansion, careful matching of duct and propeller design will be required.

With regard to the propeller design, FIG. 15 shows magnitudes of pressure reduction $p_o - p_2 = \Delta p_2$ in front of the propeller in terms of the pressure rise Δp_r across the disk and varying area ratios A_j/A_2. The pressure decrease ahead of the rotor for the expanding jet case will always be greater than the pressure rise across the rotor, as seen from FIG. 15; i.e., from Eq. 28, $p_o = p_2 + (1/2)\rho V_2^2$ and flow continuity between station 2 and jet. $\Delta p_2 = p_o - p_2$.

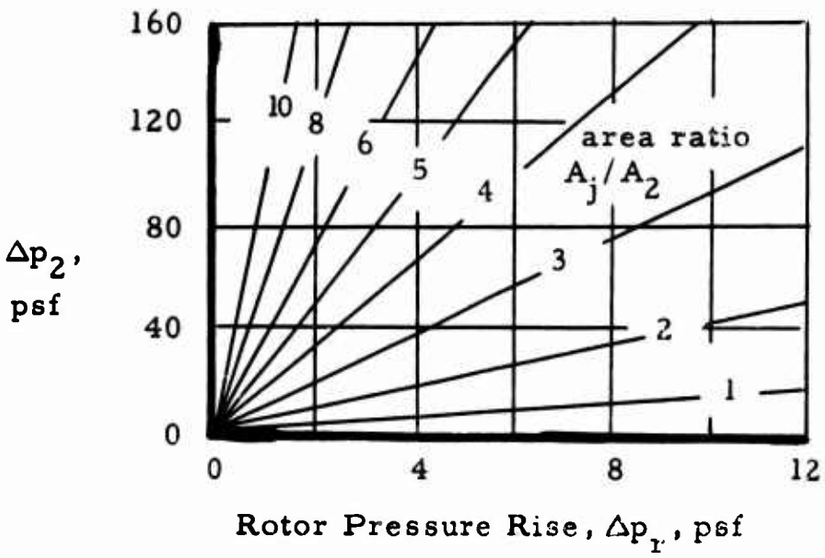

FIG. 15 RELATION BETWEEN PRESSURE CHANGES

Results on FIG. 15 follow directly from the Bernoulli equation applied to the flow upstream and downstream of the rotor.

The externally expanding flow of FIG. 13 may be difficult to reproduce physically. Jet boundary effects at the duct exit could significantly alter the ideal flow pattern. However, it might be reasoned that the known occurrence of an expanding jet behind a

helicopter in the windmill brake state* is an indication of possibly attaining a highly expanding jet; other known flows of a related nature are decelerating inflows approaching intakes and contracting exit flows in an unbounded medium. A rigorous analytical study of this case requires consideration of the duct shape and the interference effect of the jet surface on the adjacent flow field. Varying jet shape problems generally are difficult. Specific measurements related to the foregoing discussion do not seem to be available.

C. Numerical Example

As an example of the static thrust case with expanding jet, consider a required thrust of 5,000 lbs. to be produced with T/HP = 20. FIG. 11 gives A_j = 695 sq. ft. A 12.5 ft. rotor diameter leads to A_j/A_p = 5.7. Eq. 26 shows a jet velocity of 55 ft./sec. hence the axial velocity at the rotor is 314 ft./sec.

Pitch distribution for this rotor can be shown to depend, with good approximation, on the axial velocity at the rotor and the blade rpm. FIG. 16 shows several radial variations of the pitch angle for the 12.5 foot rotor. All the variations shown are compatible with the aforementioned axial velocity at the disk and in the jet.

---

*REF. 13 See photographs in Report V.1535, National Aero. Res. Inst. (Amsterdam), 1953.

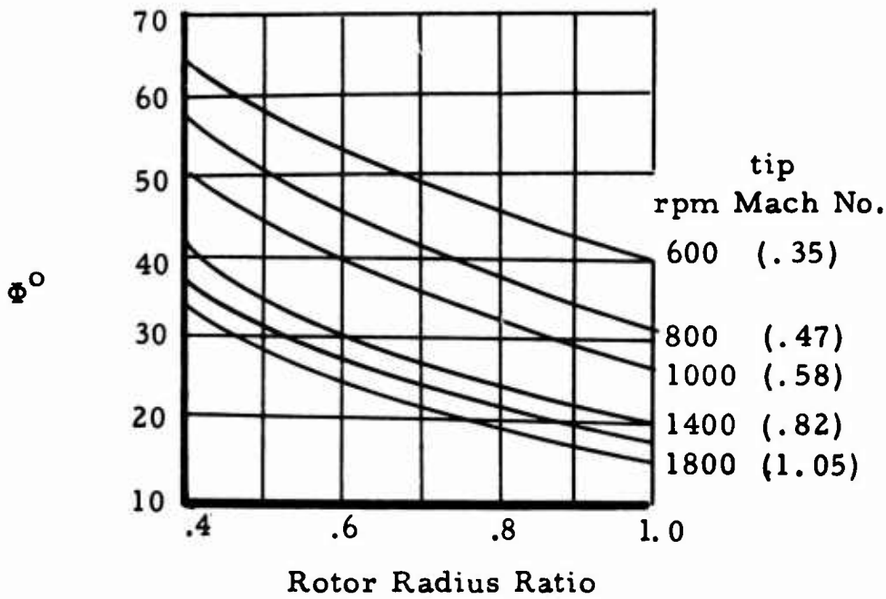

FIG. 16 EFFECT OF RPM ON DESIGN VARIATION OF PITCH ANGLE ALONG BLADE RADIUS

FIG. 16 is based on a stator located downstream of the rotor; however the effect of an upstream stator, taking account of the pre-whirl velocity, would have only a small effect on the general trends shown on FIG. 16.

The derivation of FIG. 16 is based on the fact that

$$\tan \beta = \pi nd/314 \tag{31}$$

where β is the angle between the axial direction and the relative resultant velocity approaching the blade profile. Various rpm's are selected and β calculated.

The pitch angle Φ is assumed to be approximated closely by $90-\beta$; Φ is the angle between the blade chord and the plane of rotation.

Actually $\Phi = 90-\beta+\alpha$, where α is the angle of attack between the blade chord and the relative inflow. It can be shown for the present case that α, generally, will be small compared with Φ for a blading design based on a potential or free vortex type of imparted whirl velocity; see section III.

The same power and net thrust can be produced by all the blade designs encompassed by the curves on FIG. 16. Relatively small differences may arise in the details of the blade solidity and section profile. Pitch angle difference between tip and root is about 20° for all rpms, and tends to decrease slowly with increasing rpm; pitch angles required, decrease with rotor rpm (axial velocity is the same at all rpms on FIG. 16); actual chosen rpm would depend on tip Mach number and rotational noise level; as a guide to the tip speed, πnd = 700 ft/sec occurs for N = 1069 rpm.

Pressure rise directly across the rotor for all the above designs will be less than the static pressure decrease between upstream ambient and rotor disk inflow.

For comparison with the above case, pitch angles are given on FIG. 17 for a ducted system having the same 12.5 foot rotor, but with free jet areas decreasing from the 695 sq. ft. value of this example. Shaft power for FIG. 17 is the same as used in FIG. 16. RPM for FIG. 17 is chosen at 1400. The jet area ratio curve of 5.7 on FIG. 17 is the same as the 1400 rpm curve on FIG. 16.

It is seen from FIG. 17, that as the free jet area decreases relative to the rotor disk area, the pitch angle curves show a lesser variation with radius ratio. For example, area ratio 5.7 at 1400 rpm shows about a 20° variation between tip and hub compared to 9° at area ratio 1.0.

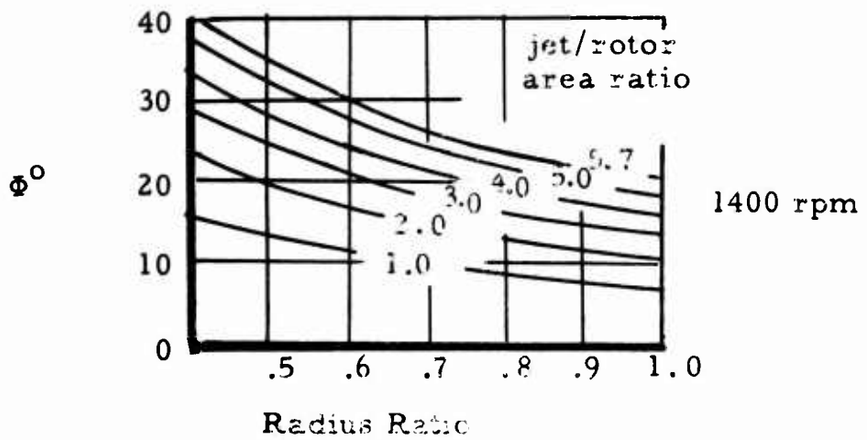

FIG. 17 EFFECT OF FREE JET/ROTOR AREA RATIO ON VARIATION OF PITCH ANGLE ALONG BLADE RADIUS

The derivation of FIG. 17 is, as stated, based on the same power input as the curves on FIG. 16. This is done by equating the power in terms of jet kinetic energy; i.e.,

$$(1/2)\ \rho\ (A_j V_j^3)_b = (1/2)\ \rho\ (A_j V_j^3)_a \tag{32}$$

where (b) denotes the values on FIG. 17 and (a) denotes the earlier values on FIG. 16. This equality, using $(V_j)_a = 55$ ft/sec, becomes

$$(V_j)_b = 55(A_j)_a/(A_j)_b \tag{33}$$

The axial velocity at the rotor is

$$V_p = (A_j/A_p)V_j \tag{34}$$

These V_p values are plotted on FIG. 18.

Knowing V_p, the β and Φ angles can be computed as denoted previously.

Also shown on FIG. 18 is the effect of the free jet/rotor area ratio on thrust/horsepower. Significant changes are seen despite the same rotor diameter for all calculations. This again implies the duct design must be compatible with these changes.

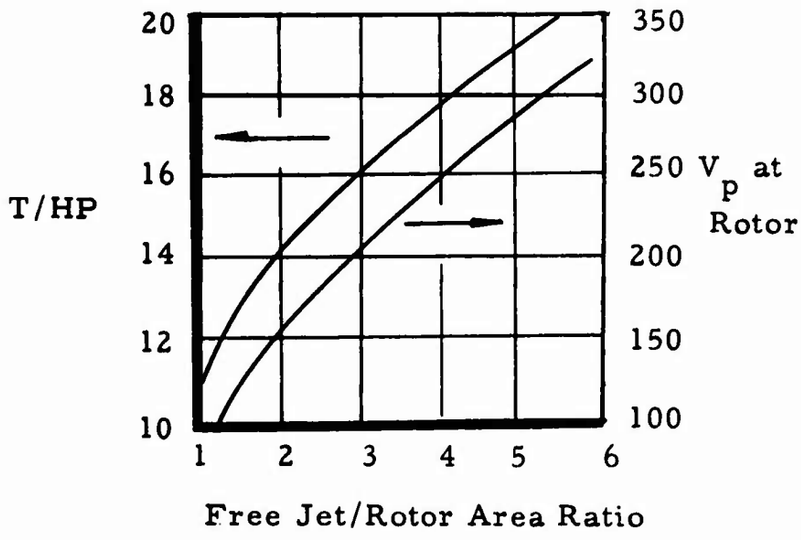

FIG. 18 EFFECT OF FREE JET/ROTOR AREA ON THRUST/HORSEPOWER AND VELOCITY AT ROTOR

III. BLADING DESIGN CONSIDERATIONS

The previous section outlines requirements for investigating ducted propeller design possibilities with high thrust/horsepower ratios. In particular, the pressure rise across rotor-stator set, force on

duct and blade pitch distribution are given for ducted systems with an expanding jet.

A further investigation of blading design in terms of solidity, lift coefficient, and/or the angle through which each profile turns the flow, is given in this present section. These results will apply to the blade design for any type of jet shape issuing from the duct. The effect of jet velocity and tip speed on blading design will also be shown in relation to (T/HP) and sonic tip speeds (noise).

In order to demonstrate blading characteristics the potential (or free) vortex type of blading design will be considered.

The power P absorbed per rotor for a free vortex design is given by the moment of momentum relation:

$$P = m \cdot \pi n d \cdot \Delta v \tag{35}$$

where:

m is the mass flow rate (ρAV)

Δv is the tangential velocity imparted by the rotor tip*

Eq. 35 can be applied to flows with or without losses, depending on the manner for determining Δv.

Considering the hovering case, the power without flow losses is given by the momentum relation:

$$P = \frac{1}{2} m V_j^2 \tag{36}$$

---

* The product $(d)\Delta v$ is radially constant for free vortex blading.

which leads to

$$\Delta v = \frac{.5 V_j^2}{\pi n d} \tag{37}$$

Eq. 37 is to be combined with the often used blade design relation:*

$$\sigma c_{L_m} = \frac{2|\Delta v|}{W_m} \tag{38}$$

where:

σ	is the solidity at a given radius
c_{L_m}	is the lift coefficient based on the mean relative resultant velocity
W_m	is the mean relative resultant velocity

FIG. 19 illustrates these quantities.

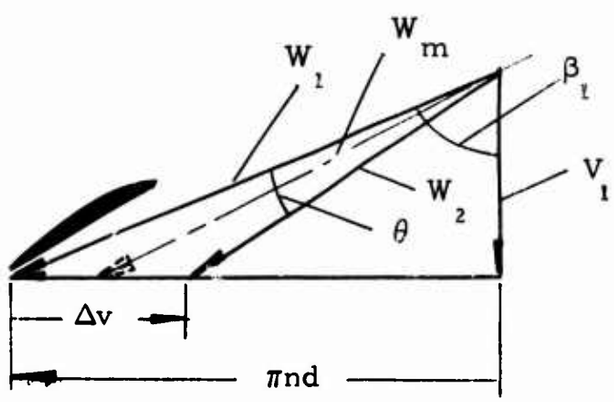

FIG. 19 VELOCITY TRIANGLE AT BLADE TIP (without upstream stator)

---

* Eq. 38 is derived by equating the differential thrust on the rotor expressed by the pressure rise, to the relation in terms of lift coefficient; the pressure rise term is subsequently replaced by the jet and upstream velocities. Eq. 38 is applicable with a stator located upstream or downstream. For an upstream stator, combined only with a rotor, the sign Δv is taken as negative; this accounts for the absolute sign shown in Eq. 38.

It is often more convenient for design work to use the stagger and turning angles β and θ, respectively, for a chosen solidity. However, for evaluating overall characteristics Eq. 38 can be very useful

The relative flow enters with velocity W_1 and leaves the blade profile at speed W_2, having turned through an angle θ and imparting tangential velocity Δv.

It is convenient to use the velocity W_1 instead of W_m since lift data suited to ducted blading usually are nondimensionalized with respect to W_1. This requires the change

$$c_{L_m} = c_{L_1} \left(\frac{W_1}{W_m}\right)^2 \tag{39}$$

which together with Eqs. 37 and 38 can be placed in the form:

$$\sigma c_{L_1} = \frac{(V_j/W_1)^2}{(W_1/W_m)} \cdot \frac{W_1}{\pi nd} \quad . \tag{40}$$

From the geometry of FIG. 19, it can be shown that

$$\left(\frac{W_1}{W_m}\right)^2 = \frac{\sec^2\beta_1}{[\tan\beta_1 - .25(A_1/A_j)^2 \cot\beta_1]^2 + 1} \tag{41}$$

and includes the continuity relation;

$$V_1 = V_j(A_j/A_1) \tag{42}$$

where:

A_1 is the annular area at the rotor disk.

A_j is the ultimate jet area.

Eqs. 40 and 41 can be placed into the sought form which applies for any radial station having the relative inflow angle β_1.

$$\sigma c_{L_1} = (V_j/W_1)^2 \{[\tan\beta_1 - .25\,(A_1/A_j)^2 \cot\beta_1]^2 + 1\}^{\frac{1}{2}} \cot\beta_1 \qquad (43)$$

Eq. 43 contains only three variables, since it can be shown from the geometry of FIG. 19 that:

$$\tan\beta_1 = \frac{\sqrt{1 - (V_j/W_1)^2\,(A_j/A_1)^2}}{(A_j/A_1)(V_j/W_1)} \,. \qquad (44)$$

The velocity ratio term V_j/W_1 is of importance to the ducted propeller for two reasons:

a) the jet velocity V_j determines the (thrust/horsepower) ratio of the entire system.*

b) the relative resultant tip speed W_1 governs the noise level of the ducted system.**

Noise levels of a ducted system should be much below that of a corresponding unducted propeller. However, for highly loaded, high rpm systems, the noise intensity will be disturbing.

Varying area ratios A_1/A_j in Eq. 43 take account of ducts with small internal area variations as well as the highly diverging free jet expansion which is predicted in section 2.

---

* It is shown on page 23 that T/HP = $1100/V_j$.

** It can be shown that the sound pressure produced for a given harmonic will vary to a power of the tip velocity.

FIG. 20 which follows is a graph of Eq. 43.

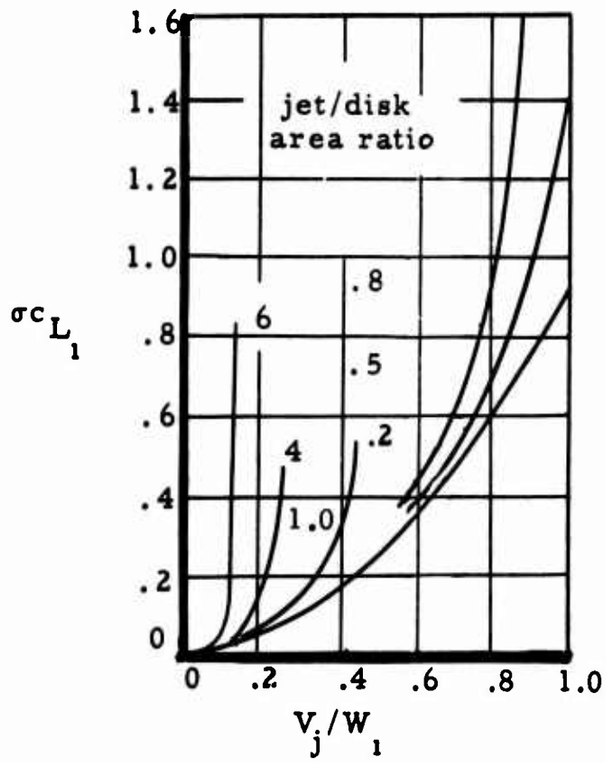

FIG. 20 BLADING CHART (any radius)

The curve for $A_j/A_1 = 1.0$ approximates the blading design of current ducted propellers; values somewhat greater than 1.0 allow for ducts with an expanding exit nozzle. Area ratios of about 2 and larger would apply for the free jet expansion described in section II or for expanding ducts having a means for preventing flow separation.

A value of V_j/W of about .1 would apply for V_j and W_1 in the order of 100 and 900 ft./sec., respectively. Velocity ratios near .1 lead to a high value of T/HP and a tip speed of 80% the sonic value. For $V_j/W_1 = 1$, FIG. 20 shows σc_{L_1} will be desirably low (<.10) over a very wide range of A_j/A_1 values. A low σc_{L_1} value implies a lightly loaded blade, which also tends to reduce the sound pressure generation.

As a guide to the limit of σc_{L_1}, it may be shown that values for σc_{L_1} of 2 and somewhat greater is near the upper limit for typical compressor blade profiles with high stagger angles ($\sim 70^{\circ}$). However, for detail design, the specific blade profile data must be used.

While the foregoing analysis can also be given in terms of the turning angle θ shown on FIG. 19, the presentation of FIG. 20 appears simpler for demonstrating the overall effects of velocity, area ratio, and velocities related to noise generation. It is possible to relate σc_L to the turning angle θ and stagger angle β at any radius. This will be done for the stator-rotor set shown on FIG. 21.

Following the methods discussed, the relation for σc_{L_1} becomes

$$\sigma c_{L_1} = \frac{\tan^2 \beta_1 - \tan^2 (\beta_1 - \theta)}{(\tan^2 \beta_1 + 1)^{\frac{1}{2}} \tan \beta_1} \quad . \tag{45}$$

Eq. 45 is plotted on FIG. 21. Highly loaded profiles, denoted by a high θ and σc_{L_1}-values, are seen to require higher stagger angles. Lightly loaded profiles can be accommodated by a much wider range of β-values.

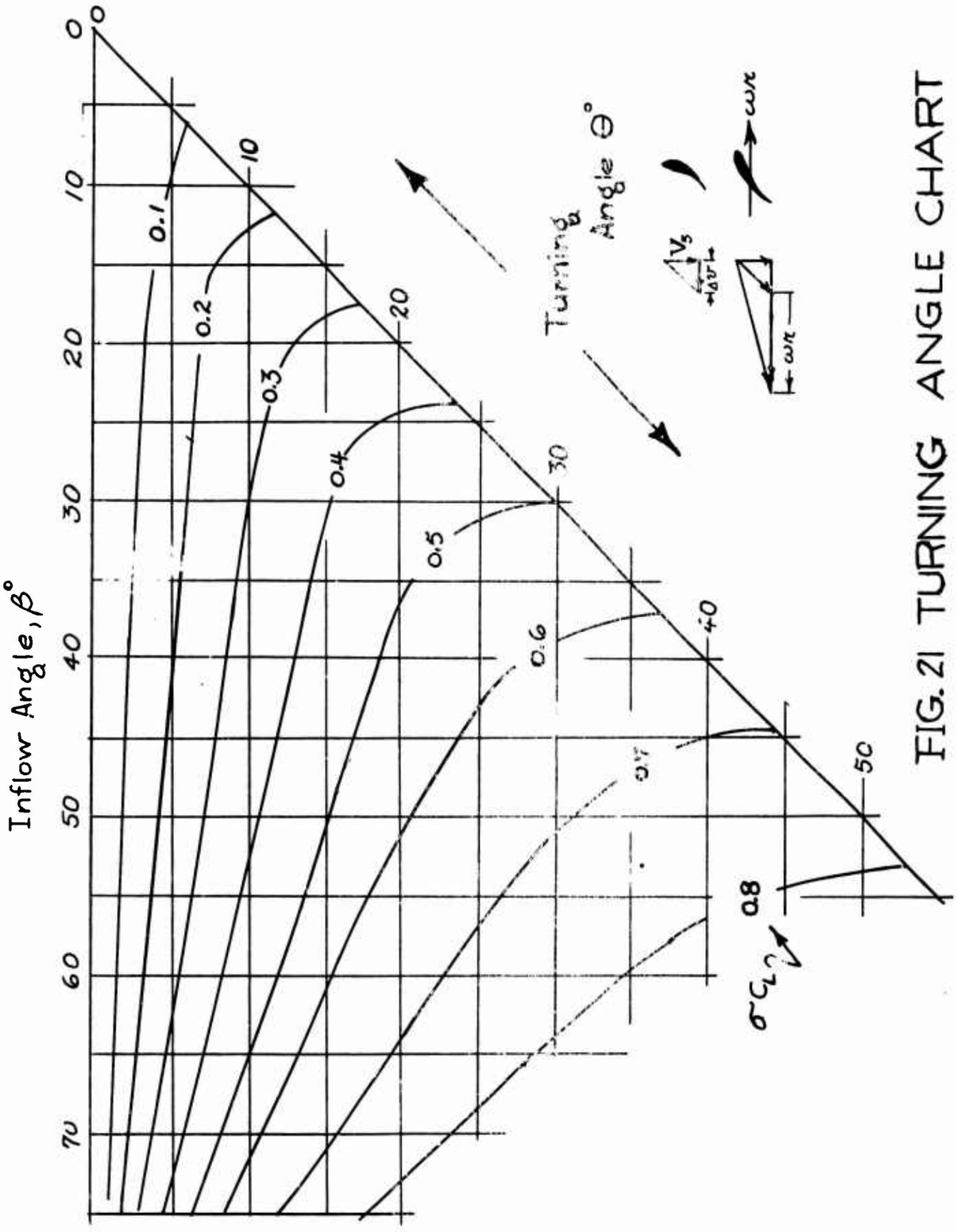

FIG. 21 TURNING ANGLE CHART

IV. ADDITIONAL DESIGN CONSIDERATIONS

A. Duct

This brief discussion concerns practical considerations currently difficult to handle by analysis. Extensive analytical work in this area is currently in progress to simplify duct selection.

It is well-known that the flow field around a duct without a propeller is generally different when the propeller is in operation. For example, a nonpowered duct having a profile with the suction side on the interior may experience a greater or lesser suction with the propeller in operation; such effects depend on the design condition of the enclosed rotor. It is also certainly to be expected that the mutual interaction of duct and rotor alters the flow field at the enclosed rotor.

The best choice for a duct length is not directly answered and can depend on several factors; e.g., inflow acceleration, pressure rise across the rotor, available length required for internal blading and aircraft stability.

Ducts which are cambered to accommodate an accelerated inflow may experience inflow difficulties at higher speeds where the inlet velocity approaches the airspeed and possibly a lower speed. For such operation it may be preferable to favor the duct inlet design for the low speed operation and incorporate a sufficient leading edge (by experience) radius to avoid intake flow separation at higher speeds. This

problem is not always resolvable in a simple manner.

Singularity techniques for studying ducted propeller flows will generally describe the characteristics of the flow field. Such techniques, which generally follow the development of REF. 14, are cumbersome in application to performance studies and it seems doubtful at this time whether this approach can be substantially improved.

Current work at ERG is seeking a rapid but highly accurate technique to obtain the flow field for designing ducted systems utilizing conventional techniques of combining mean camber lines with symmetrical profiles.

B. Tip Clearance Losses

The problem of selecting a tip clearance is one which continually occurs with ducted propeller design. Experience is an important guide for selecting a tip clearance. Studies often show the effect of blade loading on such losses. Despite this, it is interesting to note the general compilation in REF. 15 of tip losses from a wide variety of test data. A 4.6% pressure loss is shown for each 1% increase in the ratio of tip clearance/tip chord. The 100% reference point is taken at a clearance ratio of 1%.

REF. 14 Fundamentals of Annular Airfoil Theory (Nozzles In a Free Stream)(In German) by H. E. Dickman. Ingenieur-Archev, Vol.11, 1940.

REF. 15 The Effect of Tip Clearance On the Peak Pressure Rise of Axial-Flow Fans and Compressors by L.H. Smith, Jr., ASME Symposium on Stall, 1958.

C. Possible Propulsive Efficiency Improvement

The externally expanding jet considered previously for $V = 0$, can, analogously, be shown for in-flight conditions; this will be shown for the ideal propulsive efficiency e_p; without losses the familiar result in terms of the jet velocity ratio is

$$e_p = 2/[1 + V_j/V] \quad . \tag{46}$$

Eqs. 5 and 7 combine to yield

$$C_T = 2(A_j/A_e)(V_j/V)(V_j/V-1) \tag{47}$$

which yields

$$e_p = \frac{2}{1.5 + \sqrt{.25 + .5C_T/(A_j/A_e)}} \quad . \tag{48}$$

For a free propeller it can be shown that $A_j/A_e = 1.0$ with $V_j/V = 1.0$ and $A_j/A_e = 0.5$ with $V = 0$ (static thrust). FIG. 22 shows the variation of ideal efficiency with thrust coefficient and jet area ratio. Efficiency is seen to improve as the area ratio increases. Large effects are shown as the thrust coefficient increases. Design considerations to explore this possibility are the same as described in part II where the expanding jet under static operation is considered.

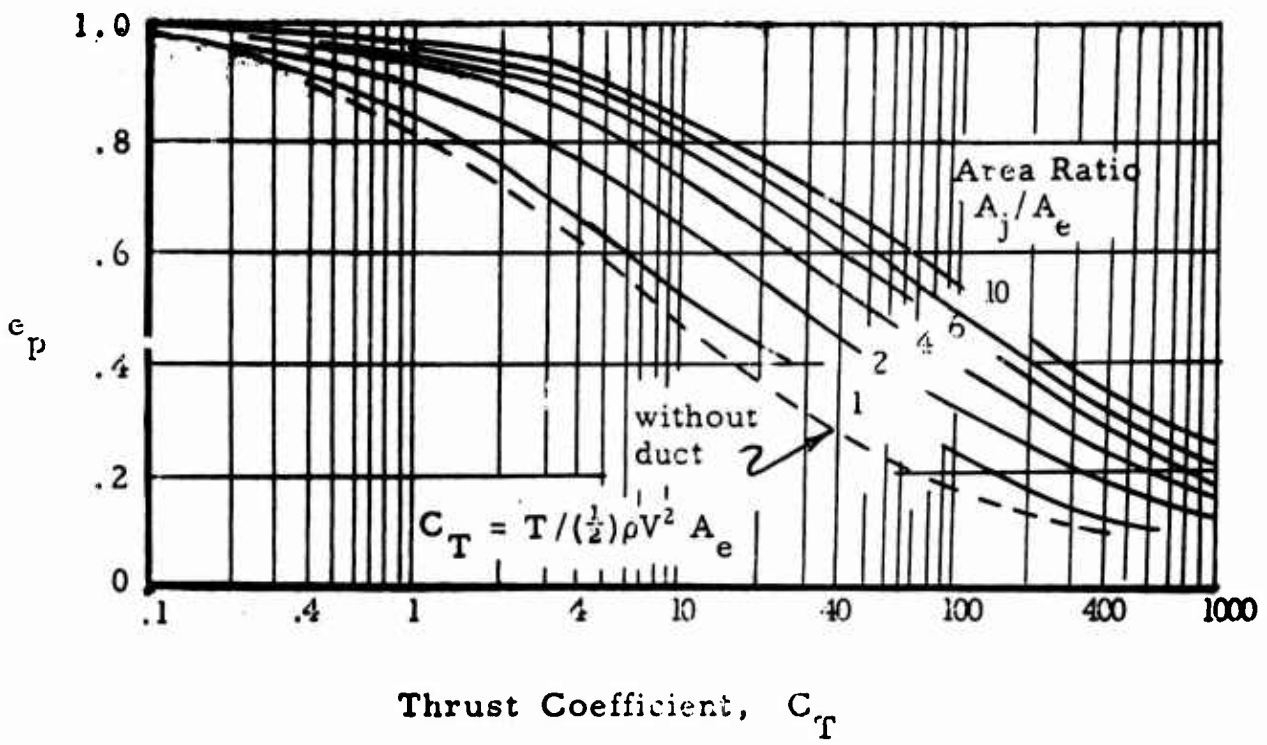

FIG. 22 **EFFECT OF EXPANDING JET ON IDEAL EFFICIENCY**

V. FLOW FIELD STUDIES

A. General

The analysis which will follow is concerned with a jet producing system located in a duct and the entire system located within a structure such as a wing or fuselage. FIG. 23 illustrates the general geometry of the jet producing system and the ambient air flow.

It is reasonable to anticipate that the inducted and ejected air flow will produce interaction or interference flows over the surrounding surfaces. Moreover the relative size of the air opening to the surrounding area can be expected to significantly influence the magnitude of the flow interference.

For example, with or without an ambient stream, an inflow which passes near to surfaces external to the duct can alter the pressure distribution on these surfaces; a similar situation will occur at the jet exit. Generally, unfavorable effects can be intuitively reasoned for the simple case of a fan-in-wing. The issuing jet can be considered as curved 'tube'. Upstream of this tube the flow will be decelerated similarly to a flow approaching a circular cylinder; this deceleration results in a pressure increase on surrounding upstream surfaces. Lower pressures should occur around the 'jet-tube' because the jet thickness and the nearby body produce a venturi type of effect to increase local velocities. The net result of the increase and decrease of pressures should depend on the strength of the vorticity related to the jet velocity ratio, but cannot be predicted without analysis or tests; however, the wing will experience a probable resulting pitch-up moment from the pressure fields, tending to reduce stability unless an additional compensating control is actuated. While this isolated example can be considered as a deleterious effect

of the interference flow, it should equally be possible to obtain a favorable effect.

A general mathematical study of the aforementioned problem requires a three-dimensional theory of the flow field around solid bodies with interference flows produced by the propulsive system having a finite size jet. Such an approach will have a wider application than the fan-in-wing case.

B. Analysis

The analysis which follows treats the three-dimensional problem of a finite size propulsive jet interacting with surrounding bodies of finite thickness. FIG. 23 illustrates the geometry.

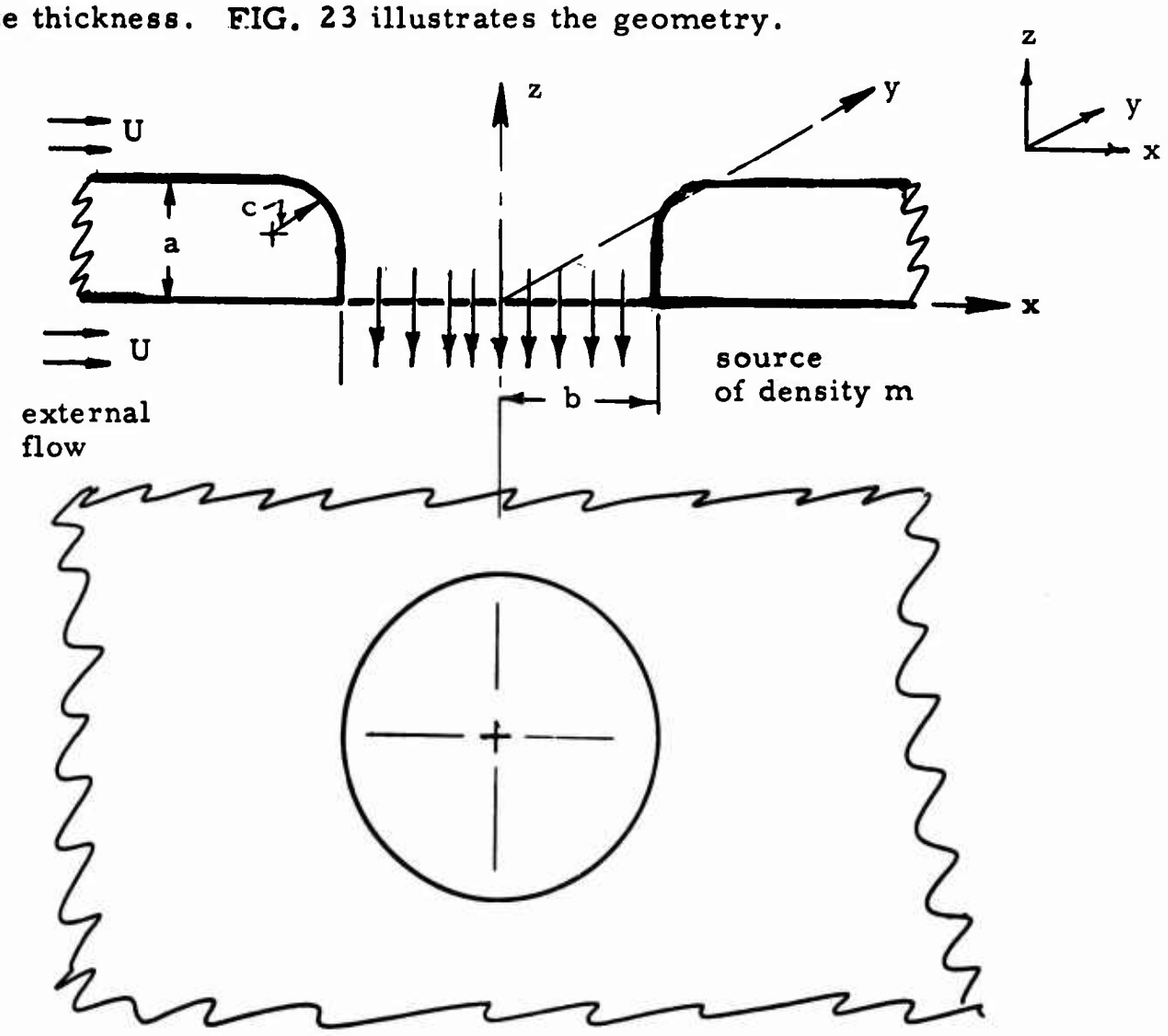

FIG. 23 FLOW GEOMETRY

Formulation of the problem is based on a source-disk flow issuing from a nozzle in an annular disk. In principle, any surrounding surface can be chosen. A uniform external flow U is superimposed as shown. The analysis seeks the potential function Φ of the entire flow field containing sources, uniform flows and a closed surface; closed surfaces generally cause mathematical difficulties. For spherical surfaces, hydrodynamical sphere theorems can be applied; this does not seem possible for the above problem. Hence, a different technique is developed as shown.

Let Φ_o denote the potential without the curved duct inlet, $\Phi_{S.D.}$ the contribution to Φ_o of the source and Φ_U the contribution of the uniform flow. Hence,

$$\Phi_o = \Phi_{S.D.} + \Phi_U \tag{49}$$

From the singularity distribution of a source disk, it can be shown that:

$$\Phi_{S.D.}(r, z) = -\frac{mb}{2} \int_0^\infty e^{-s|z|} J_1(sb) J_o(sr) \frac{ds}{s} \tag{50}$$

where J's are Bessel functions and $r = \sqrt{x^2 + y^2}$

Also, for a uniform flow:

$$\Phi_U(x, y, x) = -Ux \tag{51}$$

It is known from sphere theorems in hydrodynamics that for Φ_o, the potential of a system and $\Phi = \Phi_o + \Phi_1$ the potential after adding the closed surface S to the system, then Φ_1 is characterized completely by the following three conditions.

a) Φ_1 is regular and harmonic outside S

b) $\rho^2 \Phi_1 \to 0$ as $\rho \to \infty$; $(\rho = \sqrt{x^2 + y^2 + z^2})$ (52)

c) $\partial\Phi_1 / \partial n = -\partial\Phi_o / \partial n$ on S;)n denotes normal)

For general case of FIG. 23 the surface S consists of the surfaces (see previous figure):

(I) $z = 0,\ b \leq r \leq N$

(II) $z = a,\ b + c \leq r \leq N$

(III) $0 \leq z \leq a,\ r = N$

(IV) $0 \leq z \leq a - c,\ r = b$

(V) $a - c \leq z,\ r \leq b + c,\ (r - b - c)^2 + (z - a + c)^2 = c^2$

Condition 52 c may, therefore, be written as follows:

$$\frac{\partial\Phi_1}{\partial z}(x, y, o) = \frac{mb}{2} \int_o^\infty J_1(sb) J_o(sr) ds\ ;\ (b \leq r \leq N) \qquad \textbf{(52c, I)}$$

$$\frac{\partial\Phi_1}{\partial z}(x, y, a) = \frac{mb}{2} \int_o^\infty e^{-sa} J_1(sb) J_o(sr) ds;\ (b + c \leq r \leq N) \qquad \textbf{(52c, II)}$$

$$\frac{\partial\Phi_1}{\partial r}(x, y, a) = Ux - \frac{mb}{2} \int_o^\infty e^{-s|z|} J_1(sb) J_1(sN) ds \qquad \textbf{(52c, III)}$$

$$(o \leq z \leq a,\ x^2 + y^2 = N^2),\ \text{where}\ \frac{\partial}{\partial r} = x\frac{\partial}{\partial x} + y\frac{\partial}{\partial y}$$

$$\frac{\partial\Phi_1}{\partial r}(x, y, z) = Ux - \frac{mb}{2} \int_o^\infty e^{-s|z|} J_1(sb)^2 ds \qquad \textbf{(52c, IV)}$$

$$(o \leq z \leq a - c,\ x^2 + y^2 = b^2)$$

and

$$(r-b-c)\frac{\partial\Phi_1}{\partial r}(x,y,z) + (z-a+c)\frac{\partial\Phi_1}{\partial z}(x,y,z) =$$

$$Ux(r-b-c) - \frac{mb}{2}(r-b-c)\int_0^\infty e^{-sz}J_1(sb)J_1(sr)ds -$$

$$-\frac{(z-a+c)mb}{2}\int_0^\infty e^{-sz}J_1(sb)J_0(sr)ds \qquad (52cV)$$

$$[a-c-\leq z, r\leq b+c, (r-b-c)^2 + (z-a+c)^2 = c^2]$$

Hence, the function Φ which is sought may be characterized as the unique solution to (52c, I)-(52c, V) which is regular and harmonic outside the surface S (condition 52a) and such that:

$$\lim_{\rho\to\infty} \rho^2 \Phi_1(x,y,z) = 0 \qquad (53)$$

These are difficult equations to solve. The integrals appearing in (52c, I)-(52c, V) can be evaluated in terms of elliptic functions; however, it is doubtful that such evaluation will simplify the problem.

To review, the approach is to let $\Phi_o = \Phi_{S.D.} + \Phi_U$ be the linearized potential of the system without the closed surface S. $\Phi_{S.D.}$ and Φ_U are both known potentials. If Φ is the potential after S is added, the problem reduces to finding $\Phi_1 = \Phi - \Phi_o$; Φ_1 is subject to conditions (a), (b), (c) (page 48). The problem can be generalized to take angle of attack α by replacing Eq. 51 by

$$\Phi_U(x,y,z) = -Ux\cos\alpha - u_z\sin\alpha \qquad (54)$$

The problem as stated is to find Φ_1. Originally a solution was sought by expanding Φ_1 in a triple Fourier series and then determine the coefficients, presuming that a solution in this form exists; whether a solution exists or not, the method involves cumbersome calculations. For this type of approach, a Fourier integral method now may be more appropriate.

A more reasonable approach is to reduce the problem into two simpler problems; namely, to find two functions Φ_{11}, Φ_{12} such that

(a) Φ_{1i} is harmonic and regular outisde S, i = 1, 2

(b) $\rho^2 \Phi_{1i} \to 0$ as $\rho \to \infty$, i = 1, 2

(c 1) $\frac{\partial \Phi_{11}}{\partial n} + \frac{\partial \Phi_U}{\partial n} = 0$ on S

$\Phi_1 = \Phi_{11} + \Phi_{12}$ is then the required solution or $\Phi = \Phi_{11} + \Phi_{12} + \Phi_o$.

The problem of finding Φ_{11} involves only S and the uniform flow U; the problem of finding Φ_{12} is circularly symmetric about the z-axis.

Potential Φ_{11}

The problem is transformed to spherical coordinates (r, θ, ω) and the equation of the surface S is of the form $r = f(\theta)$. Its normal is

$$n = \frac{e_r - (\frac{1}{r}\frac{df}{d\theta})e_\theta}{\sqrt{1 + (\frac{1}{r}\frac{df}{d\theta})^2}} \tag{55}$$

Notation is shown on the sketch below

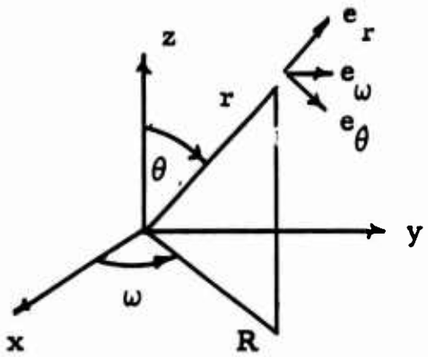

In spherical coordinates, if $\phi = \psi(r, \theta, \omega)$

$$\nabla \phi = \frac{\partial \phi}{\partial r} e_r + \frac{1}{r} \frac{\partial \phi}{\partial \theta} e_\theta + \frac{1}{r \sin\theta} \frac{\partial \phi}{\partial \omega} e_\omega$$

$$\nabla^2 \phi = \frac{1}{r^2 \sin\theta} \left\{ \frac{\partial}{\partial r}\left(r^2 \sin\theta \frac{\partial \phi}{\partial r}\right) + \frac{\partial}{\partial \theta}\left(\sin\theta \frac{\partial \phi}{\partial \theta}\right) + \frac{\partial}{\partial \omega}\left(\frac{1}{\sin\theta} \frac{\partial \phi}{\partial \omega}\right) \right\}$$

$$\Phi_U = -U(x \cos\alpha + z \sin\alpha) = -Ur(\sin\theta \cos\omega \cos\alpha + \cos\theta \sin\alpha) \tag{56}$$

$$\nabla \Phi_U = -U\{(\sin\theta \cos\omega \cos\alpha + \cos\theta \sin\alpha) e_r + (\cos\theta \cos\omega \cos\alpha - \sin\theta \sin\alpha) e_\theta - \sin\omega \cos\alpha\}$$

$$\frac{\partial \Phi_U}{\partial n} = n \cdot \nabla \Phi_U = -\frac{U}{\sqrt{1 + \left(\frac{1}{r}\frac{df}{d\theta}\right)^2}} \left[\sin\theta \cos\omega \cos\alpha + \cos\theta \sin\alpha + \frac{1}{r}\frac{df}{d\theta}(\cos\theta \cos\omega \cos\alpha - \sin\theta \sin\alpha)\right]$$

Hence the boundary condition (c2) for Φ_{11} on S is $(f^1 + df/d\theta)$ and

$$\frac{\partial \Phi_{11}}{\partial n} = \frac{U}{\sqrt{1 + (\frac{1}{r} f^1)^2}} \left[\sin \alpha \left(\cos \theta - \frac{f^1}{r} \sin \theta \right) \right. \tag{57}$$

$$\left. + \cos \alpha \cos \omega \left(\sin \theta + \frac{f^1}{r} \cos \theta\right) \right].$$

The remaining boundary conditions for Φ_{11} appear previously as (a) and (b) on page 50.

A solution is sought in the form $\Phi_{11} = F(r, \theta) G(\omega), + H(r, \theta)$. Using Laplace's equation $\nabla^2 \Phi_{11} = 0$ (in spherical coordinates) it is found that sufficient conditions on F, G, H are

$$\begin{aligned} \nabla_2^2 H &= 0 \\ \nabla_2^2 F &= \gamma^2 F/\sin \theta \\ \frac{d^2 G}{d\omega^2} &+ \gamma^2 G = 0 \end{aligned} \tag{58}$$

where γ is an arbitrary constant and the notation is

$$\nabla_2^2 [\phi(r,\theta)] = \frac{\partial}{\partial r} \left(r^2 \sin \theta \frac{\partial \phi}{\partial r}\right) + \frac{\partial}{\partial \theta} \left(\sin \theta \frac{\partial \phi}{\partial \theta}\right). \tag{59}$$

The boundary conditions (57), in terms of F, G, H on S become

$$\frac{\partial H}{\partial r} - \frac{f^1}{r^2} \frac{\partial H}{\partial \theta} = U \sin \alpha \left(\cos \theta - \frac{f^1}{r} \sin \theta\right) \tag{60}$$

$$G\left(\frac{\partial F}{\partial r} - \frac{f^1}{r^2} \frac{\partial F}{\partial \theta}\right) = U \cos \alpha \cos \omega \left(\sin \theta + \frac{f^1}{r} \cos \theta\right). \tag{61}$$

Therefore H will not present a difficulty; set

$$H = U \sin\alpha \sum_{n=1}^{\infty} a_n \frac{P_n \cos\omega}{r^{n+1}} \tag{62}$$

where the P_n are Legendre polynomials and the coefficients a_n are to be determined such that Eq. 60 is satisfied.*

G and F are still not easy to determine. The expression which will be used is $\sum_{\gamma} F_\gamma(r\theta) G_\gamma(\omega)$ where F_γ and G_γ satisfy the respective equations in Eq. 58. Hence

$$G_\gamma = b_\gamma \sin(\gamma\omega) + c_\gamma \cos(\gamma\omega) \tag{63}$$

To find F_γ the equation $\nabla^2 F = \gamma^2 F/\sin\theta$ must be solved; the family of solutions $\sin^\gamma\theta/\gamma^{\gamma+1} = F_\gamma$ are known. The approach is to take $\gamma \geq 1$ to comply with the vanishing potential at least as fast as $1/r^2$ as r becomes large. Hence the following expression can be tried.

$$U \cos\alpha \sum_{m=1}^{\infty} q_n G_n(\omega) \sin^n\theta / r^{n+1} \tag{64}$$

and determine coefficients q_n to satisfy Eq. 61. After additional solutions of the equation $\nabla^2 F = \gamma F/\sin\theta$ are found it is possible to enlarge upon this method and obtain a wider variety of infinite series available for use. For example, there should be a complimentary family of solutions to the above family.

---

* Note that for zero angles of attack, $\alpha = 0$, it follows that $H = 0$.

Potential Φ_{12}

This problem is axially symmetric; cylindrical coordinates $(R, \omega z)$ are to be used as well as the Stokes stream function Ψ. The sink disk potential $\Phi_{S.D.}$ is given previously by Eq. 50. The equation of the surface S is previously written $r = f(\theta)$, now becomes $\sqrt{z^2+R^2} = f(\arctan R/z)$ which will be written as $z = g(R)$. The sketch below is a reminder of the situation.

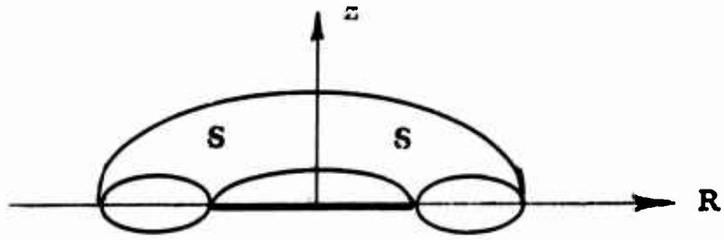

source disk

Also write $dg/dR = g^1$ and

$$\mathrm{sgn}(z) = \begin{cases} +1, & z > 0 \\ 0, & z = 0 = \epsilon \\ -1, & z > 0 \end{cases}$$

$$n = (e_R - g^1 e_z)/\sqrt{1+(g^1)^2}$$

$$\nabla\Phi_{S.D.} = \left(\frac{mb\,\mathrm{sgn}(z)}{2}\right)\left(\int_0^\infty e^{-s|z|} J_1(sb) J_0(sR)\,ds\right) e_z - \frac{mb}{2}\left(\int_0^\infty e^{-s|z|} J_1(sb) J_1(sR)\,ds\right) e_R$$

$$\frac{\partial\Phi_{S.D.}}{\partial n} = n \cdot \nabla\Phi_{S.D.} = -\frac{mb}{2\sqrt{1+(g^1)^2}}\left[\int_0^\infty e^{-s|z|} J_1(sb) J_1(sR)\,ds + \epsilon g^1 \int_0^\infty e^{-s|z|} J_1(sb) J_0(sR)\,ds\right]$$

$$= -\frac{mb}{2\sqrt{1+(g^1)^2}}\left[\int_0^\infty e^{-s|z|}J_1(sb)[J_1(sR)+\epsilon g^1(sR)]\,ds\right] . \qquad (65)$$

The boundary conditions for Ψ on S are then

$$\frac{\frac{\partial\Psi}{2z} - g^1\frac{\partial\Psi}{\partial R}}{R} = -\frac{mb}{2}\left\{\int_0^\infty e^{-s|z|}J_1(sb)[J_1(sR)+\epsilon g^1(R)J_0(sR)]\,ds\right\} . \qquad (66)$$

The equation Ψ must satisfy is

$$\frac{\partial}{\partial z}\left(\frac{1}{R}\frac{\partial\Psi}{\partial z}\right) + \frac{\partial}{\partial R}\left(\frac{1}{R}\frac{\partial\Psi}{\partial R}\right) = 0 \qquad (67)$$

noting that $\Psi \to$ constant as $r = \sqrt{R^2 + z^2} \to \infty$.

Since Eq. 67 is invariant under conformal mapping, the techniques of complex variables (two-dimensional theory) are applicable. The fact that the region S (more accurately, its intersection with the R-z plane) is not connected causes some inconvenience (it cannot be mapped into a circle). More specifically, it seems clear, intuitively, that for the sketch above, a circulation is absent around either half of S; hence, there will not be multiple valued functions involved in the potential or stream function.

From Ψ the potential Φ_{12} is obtained from the equations

$$\frac{\partial\Phi_{12}}{\partial R} = \frac{1}{R}\frac{\partial\Psi}{\partial z} \; ; \quad \frac{\partial\Phi_{12}}{\partial z} = \frac{1}{R}\frac{\partial\Phi_{12}}{\partial R} . \qquad (68)$$

The final velocity potential, as mentioned, is

$$\Phi = \Phi_{11} + \Phi_{12} + \Phi_{S.D.} + \Phi_U . \qquad (69)$$

C. Concluding Notes

The analysis presented is believed to offer a means to evaluate interaction and/or interference effects between the inflow and outflow from ducted systems and surrounding structures. It is believed that a digital computational program is needed for rapid exploration of the possibilities. Further, the techniques presented may be used to solve a wide variety of related problems. A fan-in-wing is one such problem which can be treated. For example, the method could be used for the problem of the reduced or increased pressure field on the lower wing or body surface which is developed by the interaction of the fan exit jet and free stream beneath.

VI. APPENDIX: Derivation of Eq. 3

The lift curve slope of a moderately inclined non-powered duct is given by Eq. 2. With the addition of a propeller, velocities inside and outside the same duct will change. Moreover, the change in vertical momentum component of the exit flow due to power addition must be evaluated.

Singularity technique will be applied to evaluate the new flow field and lift coefficient. The propeller may be replaced by a disk of uniform sink distribution. It is known that the effect of such a disk can also be given by a vortex distribution along the boundary of the jet stream tube. The vortex distribution induces an axially varying, circumferentially constant radial component of velocity along the duct. This radial component will alter the duct shape unless another vortex distribution is placed on the duct (cylinder) to induce an equal and opposite radial component.

Denote by $\alpha(x)$ along the duct surface the inclination of a streamline along with the horizontal and represent the physical discontinuity across the duct surface by the vortex-distribution $\gamma(x)$ along the cylinder.* By superposition of velocities, the sum of the free stream velocity V and the velocity induced by the vortex sheet must satisfy the relation:

$$\frac{V_r(x)}{V + V_x(x)} = \alpha(x) \tag{70}$$

---

* The symbol γ in this Appendix is not related to γ utilized in any preceding part of this report.

where V_r and V_x are radial and axial velocities induced by the vortices. For the assumption of a slightly curved duct surface $V > V_x$ and V_r; hence Eq. 70 becomes

$$\frac{V_r(x)}{V} = \alpha(x) \tag{71}$$

The Biot-Savart law allows $V_r(x)$ to be given by the integral

$$K\gamma(x) = V_r(x) \tag{72}$$

where $\gamma(x)$ is the vortex distribution simulating the duct.

The Kutta-Joukowski law yields the side force F on the vortex sheet; i.e.,

$$F = \int_{L/2}^{L/2} \rho V \gamma(x) R dx \tag{73}$$

The general approach is represented by the foregoing relations. In the analysis which follows the subscript (u) denotes the flow without power input; flow with power will be denoted by the same symbol with subscript (p).

The effect of power input on the lift will be derived by first seeking the counter vortex distribution which maintains the same duct shape defined by $\alpha(x)$. With power, it will be assumed that the flow inside the duct is uniform, axial and the internal velocity $V_1 \neq V$ as the general case.

A vorticity distribution γ_D is introduced to simulate the effect of the propeller on the duct. As a result γ_D axial and radial components $V_x(x)$ and $V_r(x)$ are induced along the cylinder.

Analogous to Eq. 70,

$$\alpha(x) = \frac{V_r(x)}{\overline{V} + V_x(x)} \tag{74}$$

where $\overline{V}$ is an axial velocity along the cylinder which is assumed to be essentially constant.

It is further assumed that $\overline{V}$ is the average of the velocities V and V_1 outside and inside the duct; namely:

$$\overline{V} = (1/2)(V_1 + V) \tag{75}$$

By virtue of small duct curvature and $\overline{V} >> V_x(x)$ Eq. 74 becomes

$$\alpha(x) = \frac{V_r(x)}{(1/2)(V_1 + V)} \tag{76}$$

For a given duct shape, the same boundary condition holds with or without power; this requires α (x) to be the same with or without power. Eq. 76 becomes

$$\alpha(x) = \left[\frac{K_{\gamma_o}(x)}{V}\right]_u = \left[\frac{K_{\gamma_D}(x)}{(1/2)(V_1 + V)}\right]_p \tag{77}$$

Hence the relation between the vorticities with and without power is

$$\gamma_D(x) = [(V_1 + V)/(2V)] \quad \gamma_o(x) \tag{78}$$

Inserting $\gamma_D(x)$ into the Kutta Joukowski relation (73), leads to the relation

$$F_D = [(V_1 + V)/(2V)]^2 \; F_o \tag{79}$$

where F_o is the side force without the propeller.

Eq. 79 does not give the entire side force on the duct; F_D is only the component due to the vorticity along the duct surface. In addition, the side force F_j; is to be added to take account of the vorticity along the boundary of the jet. This force is the difference between the side momentum force with and without power; viz:

$$F_j = \rho(\pi d^2/4)(V_j V_1 - V^2) \sin \alpha \tag{80}$$

for a duct at angle α.

The total side force F_p with power is

$$F_p = F_D + F_j \tag{81}$$

where the lift coefficient C_{L_p} of Eq. 3 is

$$C_{L_p} = F_p/(1/2)\rho V^2 Ld \tag{82}$$

and the unpowered lift coefficient $C_{L,u}$ of Eq. 2 is

$$C_{L,u} = F_o/(1/2)\rho V^2 Ld \tag{83}$$

Hence from Eqs. 79 through 83, together with the approximation $\sin \alpha \doteq \alpha$, Eq. 3 for $C_{L,p}$ is obtained.

VII. SYMBOLS

A	area
B	number of blades
C	blade chord
C_L	lift coefficient
$C_{L\alpha}$	lift curve slope
d	propeller diameter
e_p	propulsive efficiency
HP	horsepower
J	advance ratio, V/nd
k_L	loss coefficient
L	duct length
m	mass flow rate, (lb/sec)/g
n	rps
p	static pressure
Δp_r	pressure rise across rotor
P	power, ft lb/sec
r	blade radius
R	$d/2$
T	thrust
V	advance speed
V_j	jet velocity
Δv	whirl velocity imparted by rotor
W	relative resultant velocity
α	angle of attack
β	chord blade angle or angle of relative inflow with axial direction
σ	solidity $BC/2\pi r$
ρ	air density
λ	L/d or ωR
θ	turning angle
ω	$2\pi n$

Subscripts

1	directly upstream of rotor or average velocity inside duct with power
d	duct
e, ex	duct exit
h	hub
m	mean value
p	powered or a station in front of propeller
u	unpowered

VIII. LIST OF FIGURES

		Page
Fig. 1	Ratio of Lift Curve Slopes for Powered and Unpowered Ducts	5
Fig. 2	Geometry of Forces	7
Fig. 3	Lift of Inclined Duct (L/d = .684)	9
Fig. 4	Contracting Jet	10
Fig. 5	Lift of Inclined Duct (L/d = .5) With Operating Propeller	14
Fig. 6	Thrust Coefficient	15
Fig. 7	Jet Contraction Ratio	15
Fig. 8	Lift of Inclined Duct (L/d = .25)	17
Fig. 9	Lift of Inclined Duct (L/d = .5) With Operating Propeller	19
Fig. 10	Net Efficiency of Ducted Propeller	20
Fig. 11	Effect of Thrust/Horsepower And Jet Area on Static Thrust	24
Fig. 12	Effect of Thrust/Horsepower on Rotor Pressure Rise	25
Fig. 13	Expanding Jet Flow	26
Fig. 14	Effect of Internal Area Ratio on Duct Force	27

List Of Figures, Continued

		Page
Fig. 15	Relation Between Pressure Changes	28
Fig. 16	Effect of RPM on Design Variations of Pitch Angle Along Blade Radius	30
Fig. 17	Effect of Free Jet/Rotor Area Ratio on Variation of Pitch Angle Along Blade Radius	32
Fig. 18	Effect of Free Jet/Rotor Area on Thrust/ Horsepower and Velocity at Rotor	33
Fig. 19	Velocity Triangle At Blade Tip	35
Fig. 20	Blading Chart	38
Fig. 21	Turning Angle Chart	40
Fig. 22	Effect of Expanding Jet on Ideal Efficiency	44
Fig. 23	Flow Geometry	46

IX. BIBLIOGRAPHY

1. McEachern, N.V. Currie, M.M. — A Lifting Surface Theory For Wings With Submerged Fans. Univ. of Toronto, Inst. of Aerophysics, Decennial Symposium. 1959.

2. Moser, H.H. Livingston, C.L. — Experimental And Analytic Study of the Ducted Fan And Fan-in-Wing In Hovering and Forward Flight. Aeroelastic and Structures Research Lab. MIT TR 79-1. 1959.

3. Sacks, A.H. Burnell, J.A. — Ducted Propellers -- A Critical Review of the State of the Art. Hiller Aircraft Corporation Report ARD 232. 1959.

4. Theodorsen, Th. — Theoretical Investigation of Ducted Propeller Aerodynamics. Republic Aviation Corp. 1960. Vol. 1

5. Castles, Jr., W. Gray, R.B. — An Investigation of an Approach To The Problem of Determining The Optimum Design of Shrouded Propellers. Georgia Inst. of Technology. TREC Rept. 60-44. 1960.

6. --- --- — VTOL Aircraft Downwash Impingement Symposium U.S. Army Transportation Research Command. Ft. Eustis, Va. TREC Tech. Rept. 61-1. Dec. 1960.

X. REFERENCES

1. Fletcher, H. S. — Experimental Investigation of Lift, Drag and Pitching Moment of Five Annular Airfoils, NACA TN 4117, 1957

2. Ribner, H. S. — The Ring Airfoil in Nonaxial Flow. Jour. Aero. Sci., Vol. 14, 1947 page 529

3. Faure, M. G. — Etude Theorique De L'Aile Technique Et Science Aeronautique Tome 6, 1956

4. Weissinger, J. — Zur Aerodynamic des Ringflugeis DVL Bericht Nr. 2, 1955

5. Lippisch, A.M. — Performance Calculations of Aerodyne Systems in Cruising Flight. Collins Radio Report Cer-617, 1957. Confidential

6. Bagley, J. A. — An Estimate of the Forces on Annular Fairings. Jour. Roy. Aero. Soc., Vol. 63, 1959, page 315

7. Hoehne, V. O. — Shrouded Propeller Investigations; Wind Tunnel Tests of a Shrouded Propeller with a 10-Bladed Propeller Exit Stators and Long Chord Shroud With High Speed Inlet and No Exit Diffusion: Univ. of Witchita, Engrg. Rept. No. 213, Jan. 1959

8. Gill, W. J. — Wind Tunnel Tests of Several Ducted Propellers In Non-Axial Flow Hiller Aircraft Rept. No. ARD-224, April 1957

9. Grose, R.M. — Wind Tunnel Tests of Shrouded Propellers At Mach Numbers From 0 to 0.60. WADC TR 58-604, December 1958

10. Kuechmann, D. Weber, J. — The Flow Over Annular Aerofoils, G.D.C. 10/1133T, Ministry of Supply, British

11. Platt Jr., R.J. — Static Tests of a Shrouded and an Un-Shrouded Propeller. NACA RM L7H25. February 1948.

12. Duvivier, J. R.
McCallum, R. B.
Investigation of Large Expansion Diffusers For Minimum Rotor Area. Mass. Inst. Tech. Aero and Struct. Res. Lab. T. R. 81-1. Nov. 1959

13. ----------
See photographs in Report V. 1535 National Aero. Res. Inst. (Amsterdam) 1953.

14. Dickman, H. E.
Fundamentals of Annular Airfoil Theory (Nozzles In a Free Stream) (In German) Ingenieur--Archev, Vol. 11, 1940

15. Smith, L. H., Jr.
The Effect of Tip Clearance On the Peak Pressure Rise of Axial-Flow Fans and Compressors. ASME Symposium on Stall, 1958.